

POLITECNICO DI MILANO



Ph.D. in Hydraulics Engineering

XXIII Course

**ECOHYDROLOGICAL MODELLING OF SOIL
WATER AND NUNTRIENTS DYNAMICS IN
TROPICAL AND SUBTROPICAL BIOMES**

Tutor: Prof. Carlo DE MICHELE

Supervisor: Prof. Carlo DE MICHELE

Ph.D. Course Coordinator: Prof. Alberto GUADAGNINI

Ph.D. Dissertation of

Davide DONZELLI

Milano, January 2012

Sommario

Il presente lavoro descrive un approccio eco-idrologico allo studio delle interazioni tra cicli idrologici e biogeochimici in biomi tropical e sub-tropicali, determinati dalla disponibilità di risorse nel suolo e dalla competizione tra le componenti erbacee e arboree-arbustive che dominano tali ecosistemi.

Un primo modello si focalizza sulla competizione per acqua e azoto minerale tra tali componenti, rappresentate attraverso un sistema dinamico non lineare, che viene studiato attraverso l'analisi di biforcazione con continuazione numerica, sotto due ipotesi opposte di status competitivo, entrambe supportate in letteratura. Il comportamento del modello viene utilizzato per discriminare le due ipotesi attraverso un test statistico su un dataset di misurazioni compiute in differenti savane in Africa.

Il modello viene inoltre confrontato con i risultati di simulazioni ottenute tramite un modello biogeochimico a scala globale, e sono studiate le variazioni di produttività primaria lungo gradienti di disponibilità di queste due risorse.

Un secondo modello introduce la dinamica del fosforo nel suolo, studiando le condizioni di limitazione e co-limitazione di N e P nello stesso intervallo latitudinale. Vengono descritte la dinamica dell'acqua nel suolo e l'influenza delle condizioni di umidità sui processi di mineralizzazione delle componenti organiche di questi due nutrienti. Il comportamento del modello viene confrontato con risultati ottenuti da studi di fertilizzazione a scala regionale.

Abstract

The present work describes an eco-hydrological approach in order to analyze the interaction between hydrological and biogeochemical cycles in tropical and sub-tropical biomes, seen as ecosystems shaped by resources limitation and competition between the two dominating plant functional types of trees and grasses.

A first model investigates the tree-grass competition for multiple resources, representing the characteristics biomes succession mainly as the results of the dynamical behavior of tree and grasses competing for water and mineral in a shared volume of soil.

We use a simple dynamical resource-competition model considering two contrasting hypotheses about the behavior of tree and grasses respect to the resources: 1) tree is the superior competitor for nitrogen and grass is the superior competitor for water, and 2) tree is the superior competitor for water, and grass for nitrogen.

We study the model's properties in both the two different hypotheses, calculating steady states and bifurcations. We use data of some african savanna and a statistical analysis to select the hypothesis which better represent the data.

In addition we compare the model's results with a global simulated database finding an agreement of about 72%. Finally we study patterns of vegetation along two gradients of resources in order to investigate the potential changes of vegetation under climate variability, and patchiness of soil properties.

We develop a second model which focuses on nitrogen and phosphorous limitation in the same latitudinal range. We start from a minimal description of the dynamics of soil moisture and its interaction with the cycling of nutrients in soil, and in particular with the mineralization-immobilization turnover. We shows that, despite its parsimonius parameterization, this model is able to capture relevant characteristics of the observed patterns of nutrient limitation, in particular those obtained in nutrient enrichment experiments.

Contents

SOMMARIO	III
ABSTRACT.....	IV
CONTENTS.....	V
LIST OF FIGURES	VI
1 INTRODUCTION.....	9
1.1 OPEN PROBLEMS IN SAVANNAS DYNAMICS: AN OVERVIEW	10
1.2 PLANT-WATER RELATIONS IN TROPICAL AND SUBTROPICAL BIOMES.....	13
1.3 NUTRIENTS DYNAMICS AND PATTERNS OF RESOURCE LIMITATION.....	16
2 NUMERICAL TECHNIQUES FOR DYNAMICAL SYSTEMS	23
2.1 CONTINUATION METHODS FOR BIFURCATION ANALYSIS.....	24
2.1.1 Continuation methods in MATCONT.....	26
2.2 SIMULATION METHODS FOR NON-SMOOTH DYNAMICAL SYTEMS.....	31
3 MODELS DESCRIPTION AND ANALYSIS.....	35
3.1 TGSN MODEL: INTRODUCTION AND BIFURCATION ANALYSIS	36
3.2 SNPV MODEL: INTRODUCTION AND PARAMETER ESTIMATION	44
4 DATA COMPARISON AND RESULTS.....	49
4.1 TGSN MODEL: TESTING COMPETITION STATUS HYPOTHESES	50
4.2 TGSN MODEL: VALIDATION THROUGH A GLOBAL DATASET.....	54
4.3 TGSN MODEL: VEGETATION DYNAMICS UNDER GRADIENTS OF RESOURCE AVAILABILITY	59
4.4 SNPV MODEL: ANALYSIS OF GLOBAL PATTERNS OF NUTRIENT LIMITATION.....	62
5 CONLUSIONS AND FURTHER DEVELOPMENTS	66
5.1 INSIGHTS FROM TGSN AND SNPV MODEL.....	67
5.2 ONGOING ACTIVITIES.....	68
REFERENCES.....	70

List of figures

FIG. 1.1 DIAGRAM OF BIOME DISTRIBUTION ACCORDING TO MEAN ANNUAL PRECIPITATION AND TEMPERATURE, FROM WHITTAKER (1975), MODIFIED IN RICKLEFS (2000). THE SUBTROPICAL CATENA OCCUPIES THE RANGE OF 20°-30° OF AVERAGE TEMPERATURE AND THE FULL RANGE OF AVERAGE PRECIPITATION.	13
FIG. 1.2 A COLUMN OF SOIL WITH RELATIVE WATER FLUXES, FROM DE MICHELE ET AL. (2008).	15
FIG. 1.3 REPRESENTATION OF THE NITROGEN CYCLE IN SOILS.....	17
FIG. 1.4 NITROGEN POOLS (GN/M ²) AND FLUXES (GN/M ² /YR) AT NYLSVELEY.	19
FIG. 1.5 REPRESENTATION OF THE PHOSPOROUS CYCLE IN SOILS.	20
FIG. 1.6 PHOSPOROUS POOLS (GP/M ²) AND FLUXES (GP/M ² /YR) AT NYLSVELEY.	21
FIG. 1.7 EFFECT OF NUTRIENTS ENRICHMENT TREATMENTS ON TERRESTIAL BIOMES PRODUCTIVITY. THE RESULTS ARE EXPRESSED IN TERM OF THE LOGARITHM OF THE RATIO BETWEEN THE MESURED BIOMASS AFTER THE SPECIFIC TREATMENTS AND THE BIOMASS OF THE CONTROL PLOT. FROM ELSER ET AL 2007.	22
FIG. 2.1 THE GRAPH OF ADJACENCY FOR EQUILIBRIUM AND LIMIT CYCLE BIFURCATIONS IN <i>MATCONT</i>	26
FIG. 2.2 MOORE-PENROSE CONTINUATION.	30
FIG. 2.3 ILLUSTRATING SCHEMATICALLY TRAJECTORIES OF A PIECEWISE-SMOOTH FLOW.	32
FIG. 3.1 RESOURCE-DEPENDENT ISOCLINES FOR THE TWO FUNCTIONAL TYPE. IN HYPOTHESIS 1, $\phi_1 = \phi_T$ AND $\phi_2 = \phi_G$, WHILE IN HYPOTHESIS 2 $\phi_1 = \phi_G$ AND $\phi_2 = \phi_T$	39
FIG. 3.2 GRAPH OF INFLUENCES FOR THE STATE VARIABLES.	40
FIG. 3.3 BIFURCATION DIAGRAM OF EQ.3.7 IN THE PLANE P-Q AND NORMALIZED TREE ABUNDANCE WITHIN THE SAVANNA DOMAIN UNDER HYPOTHESIS 1. THE VALUES OF THE FIXED PARAMETERS ARE: $w_1=0.35$; $E=1.2$; $T_1=3.6$; $T_2=25.0$; $A=0.1$; $C_1=0.3$; $C_2=10.0$; $H_1=1.8$; $H_2=3.2$; $A_1=5.0$; $A_2=0.05$; $M_1=0.3$; $M_2=1.35$; $A=0.115$	42
FIG. 3.4 BIFURCATION DIAGRAM OF EQ.3.7 IN THE PLANE P-Q AND NORMALIZED TREE ABUNDANCE WITHIN THE SAVANNA DOMAIN UNDER HYPOTHESIS 2. THE VALUES OF THE FIXED PARAMETERS ARE: $w_1=0.35$; $E=1.2$; $T_1=25.0$; $T_2=3.6$; $A=0.1$; $C_1=12.0$; $C_2=0.3$; $H_1=1.5$; $H_2=2.5$; $A_1=0.05$; $A_2=5.0$; $M_1=2.9$; $M_2=0.9$; $A=2.1$	43

FIG. 3.5 SIMULATED AND MEASURED VALUES OF NORMALIZED VEGETATION DENSITY AFTER PARAMETER ESTIMATION.....	46
FIG. 3.6 SENSITIVITY ANALYSIS FOR THE PARAMETER ESTIMATED ACCORDING TO SITE SPECIFIC MASS BALANCES AT NYLSVLEY.	48
FIG. 4.1 SAMPLE ESTIMATES (DOTS) OF KENDALL'S T IN VERTICAL (TOP LINE) AND HORIZONTAL (BOTTOM LINE) SECTIONS, GROUPED FOR SOIL TYPE. THE BOX-AND-WHISKERS PLOTS REPRESENTS THE SAMPLE DISTRIBUTIONS OF KENDALL'S T UNDER THE HYPOTHESIS OF NULL ASSOCIATION (H0).	52
FIG. 4.2 GEOGRAPHICAL DISTRIBUTION OF THE SITES CONSIDERED IN THE GLOBAL DATASET.....	55
FIG. 4.3 COMPARISON BETWEEN MODEL'S PREDICTIONS AND THE GLOBAL DATASET IN THE P-Q BIFURCATION DIAGRAM. GRASSLAND (YELLOW DOTS), SAVANNA (GREEN DOTS), FOREST (BLUE DOTS) POINTS, AND THE RELATIVE 60% CONVEX HULLS (YELLOW, GREEN, BLUE LINES).....	58
FIG. 4.4 COMPARISON BETWEEN THE P-Q BIFURCATION DIAGRAM AND GLOBAL DATASET DIVIDED FOR CONTINENTS: ASIA AND OCEANIA (LEFT), AFRICA (CENTER), AND AMERICAS (RIGHT).....	58
FIG. 4.5 STEADY STATES OF TREE, GRASS, SOIL MOISTURE AND MINERALIZED NITROGEN ALONG THE PATH $P=0.18 Q$. PANEL A) SHOWS THE RESOURCE PATH ON THE BIFURCATION DIAGRAM, PANEL B) GIVES THE EQUILIBRIUM STATES FOR SOIL MOISTURE AND NITROGEN, PANEL C) ILLUSTRATES THE EQUILIBRIUM STATES FOR TREE AND GRASS.	60
FIG. 4.6 STEADY STATES OF TREE, GRASS, SOIL MOISTURE AND MINERALIZED NITROGEN ALONG THE PATH $P=0.006 Q$. PANEL A) SHOWS THE RESOURCE PATH ON THE BIFURCATION DIAGRAM, PANEL B) GIVES THE EQUILIBRIUM STATES FOR SOIL MOISTURE AND NITROGEN, PANEL C) ILLUSTRATES THE EQUILIBRIUM STATES FOR TREE AND GRASS.	61
FIG. 4.7 DISTRIBUTION OF MAP VALUES UNDER SIMULATED SITES CHARACTERIZED EITHER BY N OR P LIMITATION. BOXES REPRESENT THE INTER-QUARTILE RANGE, WHISKERS ARE THE MINIMUM AND MAXIMUM VALUES OBTAINED	63
FIG. 4.8 CONTOUR PLOT OF THE BOUNDARY BETWEEN N AND P LIMITING CONDITIONS FOR DIFFERENT MAP LEVEL.....	64
FIG. 4.9 THREE-DIMENSIONAL PLOT OF THE BOUNDARY BETWEEN N AND P LIMITING CONDITIONS. POINTS ARE FORM THE DATASET IN SANKARAN ET AL. (2005).	64
FIG. 4.10 RESULTS FROM SIMULATED 5-YEARS NUTRIENT ENRICHMENT EXPERIMENTS ON THE SAVANNAS SITE REPORTED IN SANKARAN ET AL. (2005).	65

1 INTRODUCTION

This chapter exposes a review of relevant problems concerning the dynamics of vegetation and its relation with the hydrological and biogeochemical cycles in tropical and sub-tropical biomes. Both experimental and theoretical results are reported, focusing in particular on savannas, which represent one of the most important biomes found within this latitudinal range, and are the most studied from the prospective of eco-hydrological modelling.

The main results from savannas studies will be presented, focusing on the open problems in this field of research as well. Then a synthetic description of the main processes in soil involving the hydrological cycle and the biogeochemical cycles of nitrogen and phosphorous.

1.1 Open problems in savannas dynamics: an overview

Near-tropical plant communities in which a grassy herbaceous layer coexists with a typically discontinuous woody stratum cover, broadly called ‘savannas’ (Frost et al. 1986) cover about a fifth of the global land surface (Scholes and Hall 1994). They occupy those climate regions where the rainfall is enough to permit tree growth, but there is a sufficiently long dry season that an evergreen closed-canopy forest does not develop. They are characterized by the frequent occurrence of low-intensity fires.

Such communities exhibit structural similarities in climatically similar regions of the world, independent of the vegetation history of those regions (Sankaran et al. 2008), and the mixture is apparently stable and persistent at large scales, despite high temporal and spatial variability at the patch scale. The global pattern of tree cover is predictable from environmental variables such as soil water availability, nutrient supply, fire, and herbivory (Frost et al. 1986; Bucini and Hanan 2007), as well as considerations on the history of human use. Soil moisture (i.e., the integrated effect of precipitation and evaporation) and nutrients are the key factors affecting the patterns of primary production and plant palatability to herbivores in savannas.

Savannas are second only to tropical forests in terms of their contribution to terrestrial primary production (Atjay et al. 1987). In the context of climate change, they represent a substantial terrestrial organic pool, which could act as either a net source or a sink of atmospheric carbon dioxide in future decades, depending on the path of land use and vegetation-climate feedback that may occur.

The strong and complex interactions between the woody and herbaceous plants give this biome a character of its own. While the central concept – a tropical mixed tree-grass community – is widely accepted, there is no general consensus on the precise definition of savannas, particularly on the delimitation of the boundaries.

The upper limit of tree abundance in savannas – expressed in terms of aboveground biomass, basal area, woody plant cover, or mean height – is constrained by water availability, while actual abundance at any site is often well below this limit, and is thought to reflect the disturbance history (Scholes et al. 2002, Sankaran et al. 2005).

The savannas of the world all occur in hot regions with a highly seasonal rainfall distribution. This results in a warm dry season (or two, in monsoonal climates) with a duration of three to eight months, and a hot, wet season for the remainder of the year. The rainfall seasonality occurs as a result of the latitudinal position of savannas with respect to the main tropical atmospheric circulation systems, which oscillate north and south across the savanna belt on an annual basis. The near-tropical location also implies high solar radiation. Since for much of the year there is insufficient water to absorb this energy by evaporation, it results in high temperature. The high irradiance and heat and the low

humidity combine to create a high evaporative demand, which ensures that savannas are in net water deficit for most of the year, including much of the rainy season.

Previous results (Breman and De Wit 1983; Scholes 1993) have shown that grass production in drylands, in the absence of trees, increases linearly with mean annual precipitation (a crude measure of plant available soil moisture) and that the slope of this relation is steeper when the nutrient availability is high (Vezzoli et al. 2008).

A variety of soils are found under savanna vegetation. This is attributed to the interaction of varied parent material with weathering regimes of different durations and intensities. The vegetation itself does not have a profound effect on pedogenesis in savannas, although there is often a close relationship between soil and vegetation type. Clay illuviation and ion movement are the dominant soil-forming processes, resulting in distinct soil horizons and catenary sequences. The organic matter content of savannas soils is generally low. This has been attributed to the high temperature, which lead to a high rate of organic matter decomposition, despite the fact that the water deficit in soils negatively affects this process. It is also due to the frequently sandy nature of savannas soils, and the predominance of low-activity clays, which do not encourage organic matter stabilisation. These conditions often provide soils which are deep, structureless and low in plant nutrient.

Nutrient availability, or 'soil fertility', is indexed by the clay-plus-silt content of the soil, modified in some cases by the soil depth, and is thought to be mechanistically tied to the biogeochemical cycles of nitrogen and phosphorus. As already stated, this provides a further possible link between rainfall and primary production, since the mineralization process, whereby organically-bound nutrients such as nitrogen are made available for plant uptake in mineral form, is strongly controlled by soil water availability (Scholes and Walker 1993; D'Odorico et al. 2003; Botter et al. 2008).

These factors influence in turn the kinds and extent of herbivores, associated animal impacts (Olf et al. 2002), and the frequency and intensity of fire (D'Odorico et al. 2006, Hanan et al. 2008). In the presence of trees, the grass production is usually greatly reduced, and the relationship between the grass production and the woody plant abundance is characteristically non-linear.

Even if some exceptions could occur (for example, Scifres et al. 1982, Teague and Smit 1992, in which is shown no reduction or even small increase of grass production for low tree density) the most common pattern is the following: the initial increments in woody abundance sharply reduce the grass production; but at the point where the woody abundance reaches the climate constraint line (i.e., becomes limited by tree-on-tree competition) there is typically still a small component of grass in the system (Scholes 2003).

There has been many attempts in order to represent the patterns of multiple species co-existence in terms of competition for multiple resources (Harpole and Tilman 2007, Dybzinski and Tilman 2007, Higgins et al 2010, Harpole and Suding 2011). The resource ratio theory (Tilman 1982, 1985; Dybzinski and Tilman 2007) predicts the co-existence of different vegetation species as the result of multidimensionality niches, e.g., a large number of limiting resources. Using this theory, Harpole and

Tilman (2007) have shown how the loss of grassland species is due to the reduction of niche dimensionality. Dybzinski and Tilman (2007) have investigated experimentally the pair-wise behavior of six prairie perennial plant species sharing two resources: light and soil nitrogen. Studies in desert ecosystems (Gebauer and Ehleringer 2000; Gebauer et al. 2002) have shown how the co-presence of two species of shrubs could be due to the co-limitation of water and nutrients (principally nitrogen).

Competition based models for multiple resources require the determination for each resource of the superior competitor. In tree-grass competition, a clear evidence of which is the superior competitor for water and nitrogen seems not to emerge from the literature. The case where tree is the superior competitor for the nitrogen, and grass is the superior competitor for the water, indicated hereafter as “Hypothesis 1”, or the converse, denominated “Hypothesis 2”, are both supported by experimental findings, as well as by explanations based on physiological characteristic of each functional type (tree or grass) involved. In particular Kraaij and Ward (2006) and Meyer et al. (2009) support Hypothesis 1 while Wang et al. (2010 a, b) support Hypothesis 2.

Such analyses try to identify the superior competitor of each resource using a bottom-up approach, i.e. through experimental set-ups, too local to produce generalizable evidences, or eco-physiological principles, that seem to produce questionable ad-hoc explanations.

The first model that will be presented (TGSN) has been developed in order to investigate the tree-grass competition for two resources, namely soil water and mineral nitrogen, and it will be introduced in Chapter 3.1. Stationary states are determined and their stability is discussed, focusing the attention on the domain of tree-grass coexistence (savanna stable state) and considering both Hypothesis 1 and Hypothesis 2 of competition status.

Successively, data of some african savanna (Sankaran et al. 2005) are compared to the model’s response through a statistical analysis based on the Kendall’s test of independence in order to support one of the two hypotheses against the other (or none at all). Once characterized the vegetation behavior respect to the resources, the model’s predictions are compared to a global simulated dataset, ooutput of a biogeochemical spatially distributed model, applied over all the earth surface.

Two transects along different gradients of precipitation and nitrogen are considered in order to investigate the potential changes in vegetation structure under climate variability, or changes, and patchiness of soil properties.

The second model (SNPV) has been developed in order to investigate pattern of resource limitation (nitrogen and phosphorous) through a minimal model (Chapter 3.2). The paucity of data on P limitation and the fact that a combined analysis of both nutrients is absent in most terrestrial biogeochemical modles such as CENTURY (Parton et al. 1987) requires some theoretical effort in order to address the significance of such interaction. In this model, we neglect resource competition between different plant functional types, but we address the influence of the hydrological cycle on nutrient availability on time scales that are relevant for vegetation dynamics.

1.2 Plant-water relations in tropical and subtropical biomes

The strong association between and climates with a hot, wet summer and a warm, dry winter provides the first clue that water availability is a key factor of the ecology of tropical and subtropical biomes. The dominance of water availability as a determinant of biomes structure and function is particularly strong at the dry end of the savanna spectrum, and it has a key role in shaping the peculiar succession of biomes along an aridity gradient, known as *subtropical catena* (Fig. 1.1), that is characteristic for the vegetation structure across the different continents.

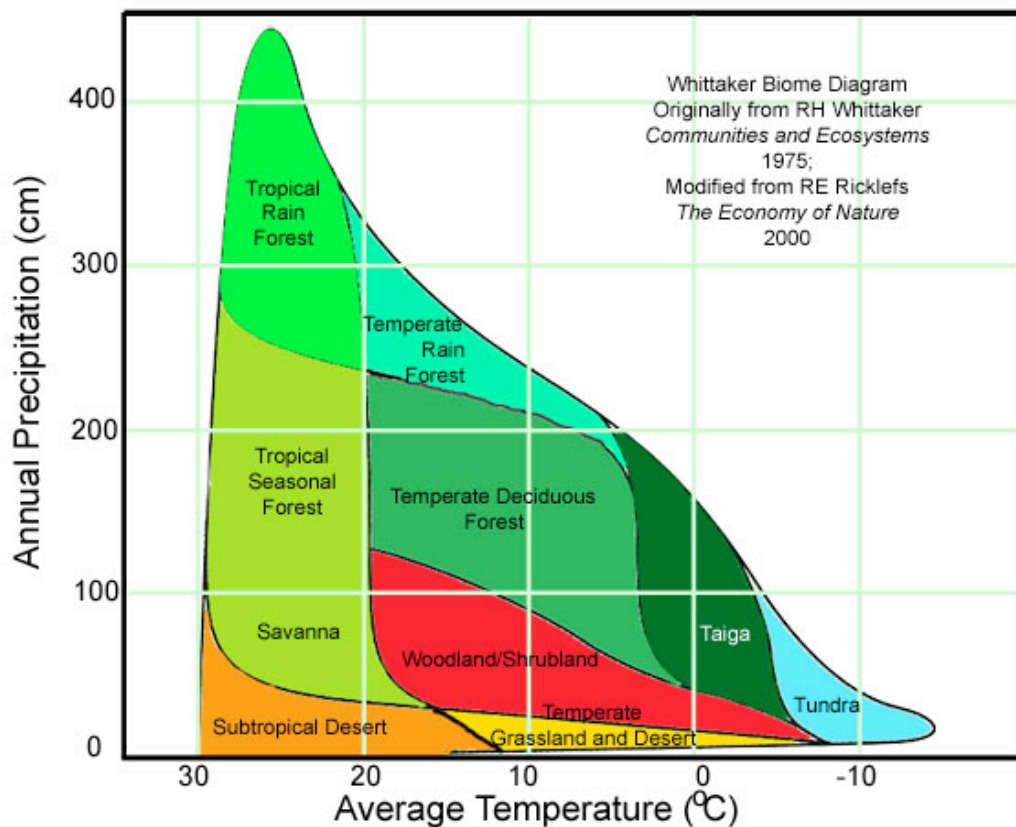


Fig. 1.1 Diagram of biome distribution according to mean annual precipitation and temperature, from Whittaker (1975), modified in Ricklefs (2000). The subtropical catena occupies the range of 20°-30° of average temperature and the full range of average precipitation.

The pattern of water supply in relation to the water requirements of the plants influences both the physical vegetation structure and their ecological composition. An observer passing down the aridity

gradient from a moist savanna, receiving perhaps 1000 mm rainfall per year, into a desert shrubland or grassland receiving 300 mm rainfall per year will be struck by the progressive decrease in the height and density of the trees, and the consequent change in the proportion of trees to grasses. A similar change can be noted when passing across variation of soil texture under the same climate and is due, in part, to the different hydrological characteristics of soils.

The obviousness of the importance of water in savannas can sometimes be a hindrance to understanding their ecology, since it conceals the importance of other more subtle factors. Water availability determines savanna function by controlling the duration of the period for which processes such as primary production and nutrient mineralization can occur. Walter (1971) first noted the monothonic increasing relationships between annual rainfall and grass production in the dry savannas of Namibia, and similar relationships have been documented in many parts of the world.

The terrestrial hydrological cycle is controlled by many interacting factors, including climate, soil conditions and plant characteristics. Since most of these factors are difficult to measure on a continuous basis and at the appropriate spatial scale of aggregation, the most practical way to explore their importance is within the framework of a simulation model that incorporate the key process of the cycle: runoff, infiltration, deep drainage, interception by leaves and subsequent evaporation, evaporation from soil and of transpiration by plants (Fig. 1.2).

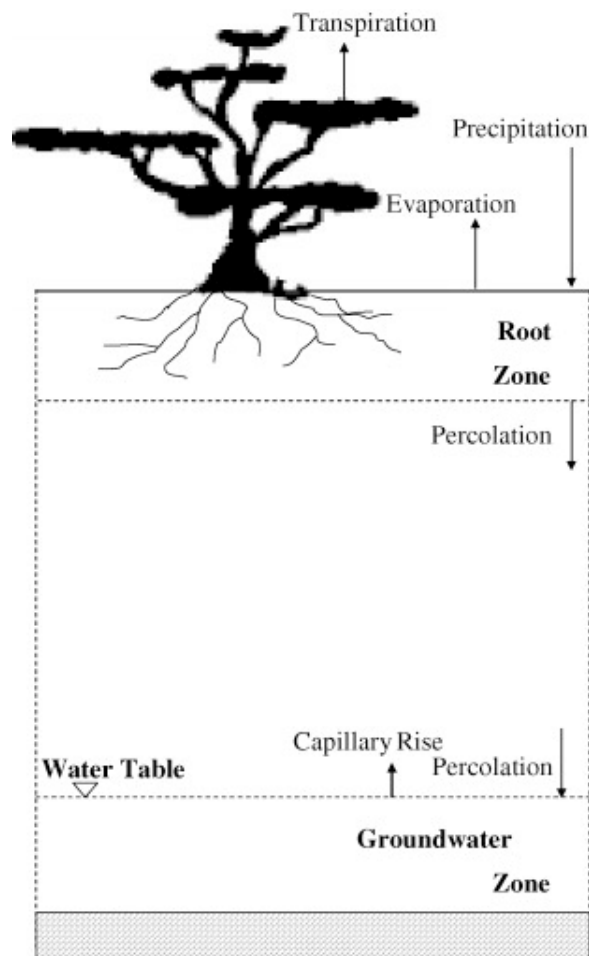


Fig. 1.2 A column of soil with relative water fluxes, from De Michele et al. (2008).

In Accatino et al. (2010) it is shown through a simplified hydrological model how the *sub-tropical catena* can be interpreted in term of the interaction between soil water competition and vegetation disturbances like fire.

For $100 \leq p \leq 600$ mm/y the dry savanna co-existence is permitted by the balanced competition for limited rainfall and fire influences only the tree-grass ratio. The system would still be a savanna, even in the absence of fire. For rainfall above 1100 mm/y the moist savanna co-existence can only occur in the presence of a high level of fire disturbance, because the ecosystem would be a forest in the absence of fire. In the intermediate range, $600 \leq p \leq 1100$ mm y-1, savanna is the result of the co-occurrence of water limitation and fire.

The model shows how dry savannas are stable equilibria, while moist savannas are a bi-stable condition with forest, and it also allows to predict the vegetation structure changes that occur along gradients of rainfall and fire frequency, and to clarify the distinction between climate-dependent ecosystems and fire-dependent ecosystems (Bond and Keeley 2005).

1.3 Nutrients dynamics and patterns of resource limitation

In this chapter we concentrate on the movement of two key elements – nitrogen and phosphorous – not as energy carriers, but as building blocks essential for the growth of any organism. It is useful to examine the pathways of nitrogen and phosphorous against the background of the carbon cycle, since for the major biological portion of their cycles they are found in organic form (that is, as part of carbon-based molecules). Among the key processes regulating the passage of N and P through the ecosystem is the process whereby they are liberated from their carbon bondage, and become available for uptake by the organisms.

The trademark of systems ecology is a flow diagram consisting of boxes and interconnecting arrows. The boxes represent reservoir or pools of a particular element, and the arrows show the rate and direction of transfer (flux) of the element between pools. The fluxes are usually inferred from the rate of change in the size of their source or sink pools, although some fluxes can be measured through specific techniques (for example, incubation of soil sample) as we will see in the following. Identifying and quantifying the fluxes is a considerable improvement beyond a static representation of the pools sizes, but a complete biogeochemical system analysis requires knowledge of the factors which control the rate of the flux, as well.

The pathways of carbon, nitrogen and phosphorous are strongly associates, and they form an interesting continuum from a very open cycle (carbon) to a tightly closed one (phosphorous), with nitrogen in between. The carbon cycle has large fluxes to and from the atmospheric carbon pool which is defined as being outside of the system. Therefore, at the scale of a patch of vegetation, the carbon cycle is ‘open’. The nitrogen cycle also include an atmospheric loop, but it is small relative to the recycling which occurs within the plant-soil system. Phosphorous cycling is virtually entirely restricted to the plant-soil system, since atmospheric fluxes are generally neglectible, and it differs from the nitrogen cycle in the prominence of the inorganic soil pools and the non-biological processes of exchange between them. The degree of ‘openness’ of the cycle has important consequences on the potential for loss of elements from the system, and on the rate of recovery after such leakage.

Nitrogen and phosphorous are essential for the growth and functioning of all organisms, and their availability is a potential constraint on productivity. Since they are required in large quantities relative to ther elements, they are classified as ‘macronutrients’, being the most frequently limiting nutrients in terrestrial ecosystems.

Now the two cycles of nitrogen and phosphorous will be described in details. The terrestrial N cycle comprises soil, plant and animal pools that contain relatively small quantities of biologically active N, in comparison to the large pools of relatively inert N in the litosphere and atmosphere, but that nevertheless exert a substancial influence on global biogeochemistry, due to the relatively ‘closeness’ of this cycle in relation. After carbon (ca. 400 g/kg) and oxygen (ca. 450 g/kg)m N is the next most abundant element in plant dry matter, typically 10-30 g/kg. It is a key component of plant amino and

nucleic acids, and chlorophyll, thus directly influencing plant productivity, and is usually acquired by plants in greater quantity from soil than any other element.

The largest N pool in the plant root zone is in the soil organic matter, but this is mostly unavailable to plants. However, this organic N may be released (mineralised) to form plant-available or mineral N. Organic matter decomposition is a complex process that occurs, to differing extent, with newly added plant residues, animal waste products, root exudates and rhizodeposits as well as various existing or 'native' soil organic pools. This results in a continuum of organic materials of varying ages, stages of decay and degree of recalcitrance. Decomposition is mediated largely by soil biota and results ultimately in release of nutrients in mineral form and loss of C from the soil as CO₂ via respiration. The microbial biomass has a pivotal role in the soil N cycle (Fig. 1.3) and was aptly described by Jenkinson et al. (1990) as "the eye of the needle through which virtually all nutrient must pass".

The continuous transfer of mineral N into organic materials via incorporation into soil microbial biomass, and the subsequent release back into the soluble mineral N pool is known as "mineralization-immobilization turn-over" or MIT (Jansson and Persson 1982), and it is considered to play a dominant role in the availability of N for plants in natural ecosystems.

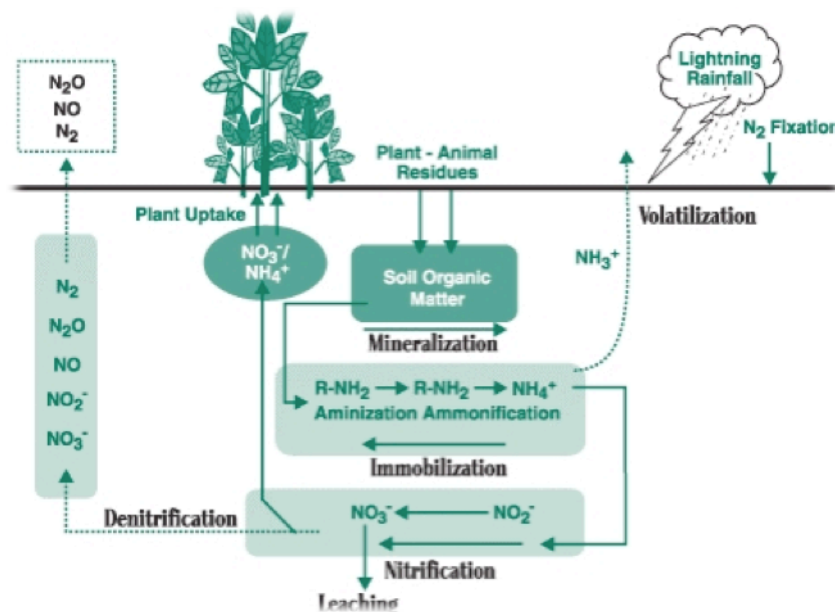


Fig. 1.3 Representation of the nitrogen cycle in soil, from Marschner and Rengel (2007).

Gross N mineralization in soil results in the release of ammonium (NH_4^+) or ammonia (NH_3) by non-specific heterotrophic soil micro-organism under aerobic and anaerobic conditions. The bulk of N mineralization occurs in the biologically active surface soil that contains most of the dead and decomposing litter. The process of gross N immobilization involves microbial assimilation of NH_4^+ and, to a lesser extent, NO_3^- .

As stated before, it has proved far easier to measure the net effect in soils of MIT, rather than gross immobilization and mineralization, by simply analysing temporal changes in inorganic N over defined period, whilst minimising or taking into account losses or gains. The available approaches range from laboratory incubations to large-scale field studies (Marschner and Rengel 2007).

Ammonium in soil may be oxidised via nitrite (NO_2^-) to NO_3^- at a rate regulated primarily by availability of NH_4^+ . This process, called nitrification, can be autotrophic or heterotrophic, and from the relatively small number of microbial species involved, it is greatly influenced by edaphic factors such as pH, moisture, temperature and aeration.

Plants may acquire N from soil as NH_4^+ , NO_3^- or NO_2^- , and the uptake is an increasing function of the respective concentrations in the soil solution, being also influenced by root distribution and soil water content. The concentration of N in plant dry matter of herbaceous plants is typically 10-20 g/kg for grasses and forbs, and 20-30 g/kg for legumes, due to the effect of mycorrhizae symbiosis in fixing atmospheric nitrogen, and tends to be higher in younger tissues. For woody plants, the concentration of N varies with plant parts, typically being <5 g/kg for woody tissue and <20 g/kg for leaves, due to the resorption of available nutrients from dying leaves.

Among the losses that characterise the N cycle, leaching is the most relevant for its connection with the hydrological cycle. The two major determinants of this process are the quantity of water passing through the soil profile and the concentration of soluble elements at that time. Thus leaching occurs whenever mineral N accumulation in the soil solution coincides with, or is followed by, a period of high drainage.

Ecosystem disturbances caused by fire, harvest, cultivation and grazing tend to increase the potential for leaching in both natural and agricultural systems. Reported quantities of mineral N leached vary enormously within similar ecosystems and even more widely between different ones.

Overall, leaching is exacerbated on light sandy soils, and tend to be much larger in agrosystems that are frequently disturbed. However, the extent and scale of losses, particularly of the most labile organic part of the soil N pools, via leaching in natural ecosystems is still relatively unknown and, despite acknowledgement that these losses may comprise a significant part of the terrestrial N cycle, there is a paucity of quantitative information on it. In order to give some order of magnitude for the processes involved, Fig. 1.4 shows the N cycle at the Nylsvley savannas site in South Africa (Scholes and Walker 1993).

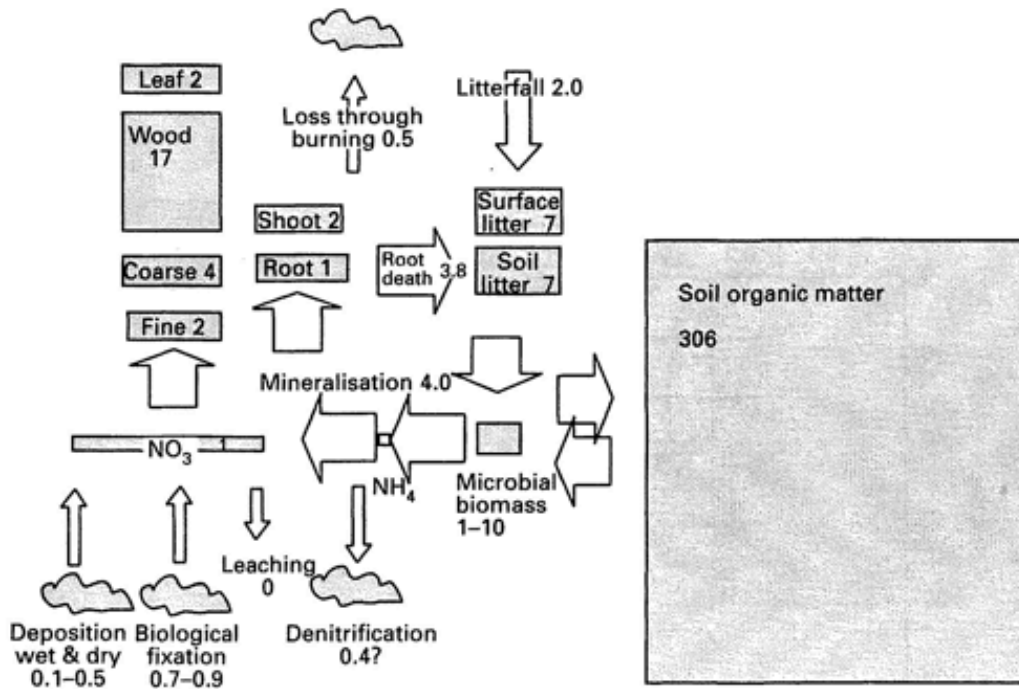


Fig. 1.4 Nitrogen pools (gN/m²) and fluxes (gN/m²/yr) at Nylsveley, from Scholes and Walker (1993).

The cycle of P in the plant-soil difference presents some peculiarities with respect to the N cycle (Fig. 1.5). The low solubility of inorganic phosphorous compounds is an important factor in the cycle, consequently the soil P is conceptually viewed as consisting of a small readily available exchangeable pool, a moderately available labile pool, and a large, unavailable occluded pool, all in equilibrium with one other.

The chemical reality is a little more complex, since phosphorous is present in a large variety of forms in the soil, and these forms do not fit neatly into the three conceptual boxes. Organic P is in the soil organic matter and microbial biomass, and is released by microbial oxidation in the same way that nitrogen. The byproduct of net mineralization can react to form calcium, aluminium or iron phosphates, which can be occluded by iron and aluminium oxides, preventing their solubilisation and leading to inorganic pools that are not directly available to plant uptake. On the other hand, low solubility leads to losses from leaching that are far more neglectible than the nitrogen counterpart.

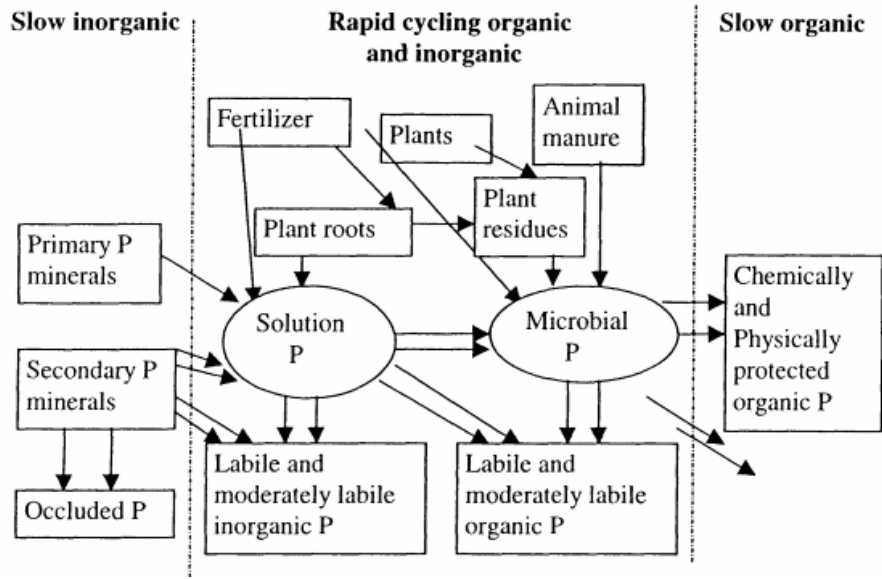


Fig. 1.5 Representation of the phosphorus cycle in soil, from Marschner and Rengel (2007).

Despite sharing an almost equivalent role in limiting the productivity of terrestrial ecosystems, the P cycle is even less studied in a quantitative way than the N cycle. This is partly due to the impossibility of using incubation methods to measure the net mineralization of organic P and consequent release of mineral soluble P by soil biota. In fact, laboratory incubation conditions lead to sorption of the end phosphate product, preventing the reliability of the measurement of mineral P concentration at the end of the process and making more difficult the assessment of releases in soils of available P. Furthermore, the presence of pools of inorganic P that are unavailable to plants complicates the interpretation of the measurement of total P, since those pools can act as either a source or a sink of phosphorus. As for the N cycle, Fig. 1.6 shows the size of pools and fluxes at Nylsvey.

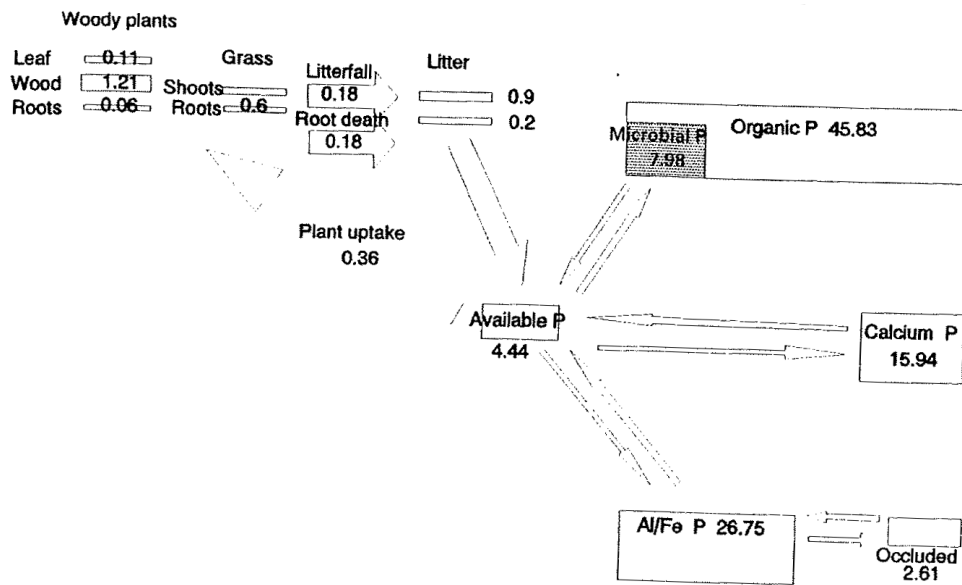


Fig. 1.6 Phosphorous pools (gP/m²) and fluxes (gP/m²/yr) at Nylsveley, from Scholes and Walker (1993).

Past work has highlighted a diverse set of geochemical and ecological factors that can influence the identity and nature of N and P limitation in particular ecosystems (Vitousek and Howarth 1991). In terrestrial environments, soil age is a key factor because P becomes increasingly sequestered via mineralogical transformations occurring over time scales of 10³-10⁵ years (Walker and Syers 1976, Vitousek 2004). Thus, tropical ecosystems that were not disturbed by glaciation are thought to be more frequently P-limited because of greater soil age.

On the other hand, regional fire regime can also have a major impact, as fire volatilizes N pools while leaving P behind (Raison 1979, Hungate et al 2003). This diversity of habitat-specific climatic, edaphic and ecological influences on N and P availability make it difficult to obtain a broad picture of their relative importance as limiting resource in the biosphere.

Nevertheless, some existing paradigms identify N as the primary limiting nutrient, while recent work has begun to question this generalization, calling attention to an equivalence of N and P limitation over a broad set of ecosystems.

An interesting meta-analysis of different experimental enrichments, carried out in Elser et al. (2007), which shows substantial variation in nutrient response within terrestrial ecosystems, with pattern of co-limitation broadly similar across different subhabitat, while P limitation appears to be more frequent in forests and shrublands, and N and P limitation seem to be equally distributed in grassland biomes (Fig. 1.7).

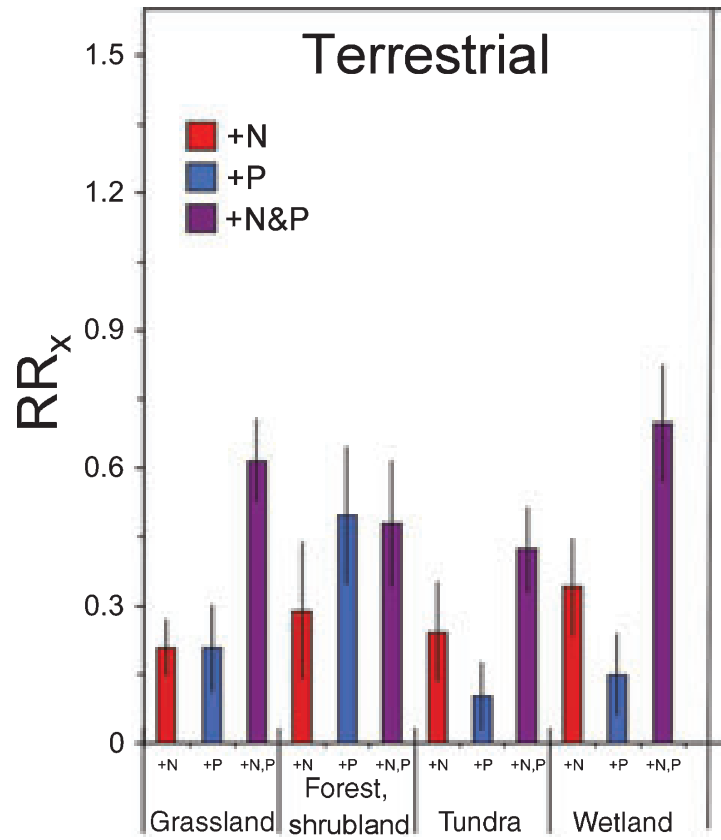


Fig. 1.7 Effect of nutrients enrichment treatments on terrestrial biomes productivity. The results are expressed in term of the logarithm of the ratio between the mesured biomass after the specific treatments and the biomass of the control plot. From Elser et al. (2007).

2 NUMERICAL TECHNIQUES FOR DYNAMICAL SYSTEMS

In this chapter will be presented a review of numerical techniques used for the analysis of dynamical systems. Such techniques will be used for studying the eco-hydrological models presented in the following chapter. In particular, we are interested in understanding the qualitative behaviour of a particular system depending on the variations of a small set of free parameters, that is a bifurcation analysis. We will start in the context of smooth non-linear dynamical systems, for which it exists a well assessed classification of bifurcation modes, and numerical tools to detect them. Then we will deal with non-smooth dynamical systems, that represent a rich and active field of research, and an algorithm for accurate direct numerical simulations of such systems will be presented. This introduction does not claim to be an exhaustive description of these topics, that are subject of still ongoing researches. Our objective is to introduce the reader in some techniques extensively used for the analysis of the ecohydrological models which represent the main contribution of this work.

2.1 Continuation methods for bifurcation analysis

Consider an autonomous system of ordinary differential equations (ODEs)

$$\dot{x} = f(x, \lambda) \quad x \in R^n, \lambda \in R^p \quad (\text{Eq.2.1})$$

where f is smooth. A bifurcation occurs at parameter $\lambda = \lambda_0$ if there are parameter values λ_1 arbitrarily close to λ_0 with dynamics topologically inequivalent from those at λ_0 . For example, the number or stability of equilibria or periodic orbits of f may change with perturbations of λ from λ_0 . One goal of bifurcation theory is to produce parameter space maps or bifurcation diagrams that divide the λ parameter space into regions of topologically equivalent systems. Bifurcations occur at points that do not lie in the interior of one of these regions. Bifurcation theory provides a strategy for investigating the bifurcations that occur within a family. It does so by identifying ubiquitous patterns of bifurcations. Each bifurcation type or singularity is given a name.

Associated with each bifurcation type are

- defining equations that locate bifurcations of that type in a family $\dot{x} = f(x, \lambda)$
- normal forms that give model systems exemplifying the bifurcation type

Inequalities called non-degeneracy conditions are part of the specification of a bifurcation type. The bifurcation types and their normal forms serve as templates that facilitate construction of parameter space maps. Bifurcation theory analyzes the bifurcations within the normal forms and investigates the similarity of the dynamics within systems having a given bifurcation type.

One can view bifurcations as a failure of structural stability within a family. A starting point for classifying bifurcation types is the Kupka-Smale theorem that lists three generic properties of vector fields:

- hyperbolic equilibrium points;
- hyperbolic periodic orbits;
- transversal intersections of stable and unstable manifolds of equilibrium points and periodic orbits.

Different ways that these Kupka-Smale conditions fail lead to different bifurcation types. Bifurcation theory constructs a layered graph of bifurcation types in which successive layers consist of types whose defining equations specify more failure modes. These layers can be organized by the codimension of the bifurcation types, defined as the minimal number of parameters of families in which that bifurcation type occurs. Equivalently, the codimension is the number of equality conditions that characterize a bifurcation.

One of the principal uses of bifurcation theory is to analyze the bifurcations that occur in specific families of dynamical systems. Investigations commonly identify the types of bifurcations in parameter space maps either by comparison of simulation results with normal forms or by solving defining equations for those bifurcation types in the systems under investigation and computing coefficients of the normal forms. Several software packages (AUTO, CONTENT, MATCONT, XPPAUT, PyDSTool) give implementations of algorithms that perform the latter type of analysis. The numerical core of these packages consist of

- regular implementations of defining equations for the bifurcation types;
- equation solvers such as Newton's method;
- numerical continuation methods for differential equations;
- computation of normal forms;
- initial and
- boundary value solvers for differential equations.

The continuation methods compute curves of solutions to regular systems of N equations in $N+1$ variables. The bifurcation analysis of a system implemented to varying degrees in the packages listed above is based upon the following strategy:

- an initial equilibrium or periodic orbit is located;
- numerical continuation is used to follow this special orbit as a single active parameter varies;
- defining equations for codimension one bifurcations detect and locate bifurcations that occur on this branch of solutions;
- starting at one of the located codimension one bifurcations,

two parameters are designated to be active and the continuation methods are used to compute a curve of codimension one bifurcations.

- defining equations for codimension two bifurcations detect and locate bifurcations that occur on this branch of solutions;
- starting at one of the located codimension two bifurcations,

three parameters are designated to be active and the continuation methods are used to compute a curve of codimension two bifurcations.

This process can be continued as long as one has regular defining equations for bifurcations of increasing codimension, but these hardly exist beyond codimension three. Moreover, the dynamic behaviour near bifurcations with codimension higher than three is usually so poorly understood that the computation of such points is hardly worthwhile. In many cases, bifurcation analysis identifies additional curves of codimension k bifurcations that meet at a codimension $k+1$ bifurcation. Continuation methods can be started at one of these codimension k bifurcations to find curves of this type of bifurcation with $k+1$ active parameters.

2.1.1 Continuation methods in *MATCONT*

MATCONT is a freeware continuation toolbox developed under *MATLAB* environment, which is able to detect bifurcations of equilibrium, limit cycle and homoclinic orbit up to codimension 2 (Fig. 2.1 and Tab. 2.1).

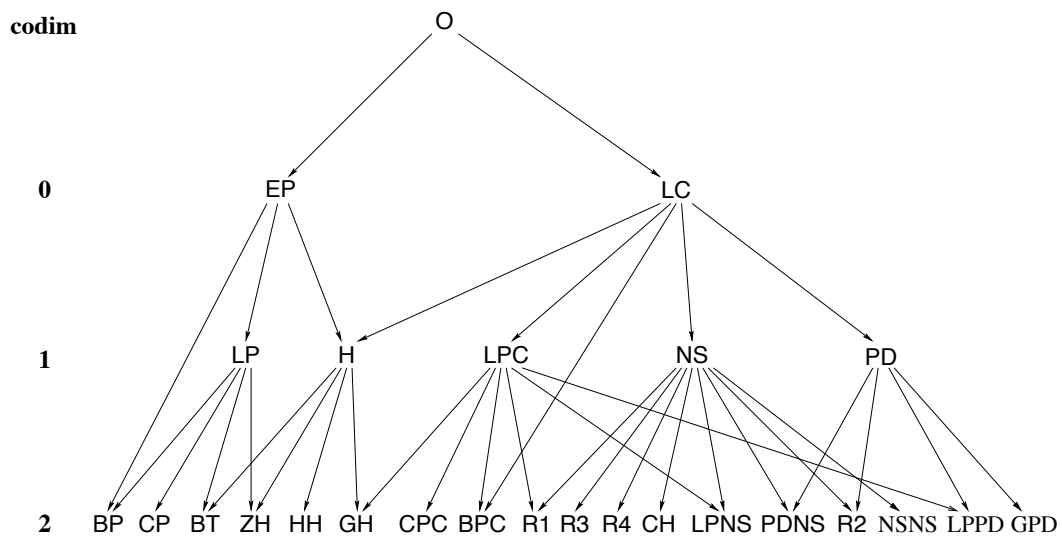


Fig. 2.1 The graph of adjacency for equilibrium and limit cycle bifurcations in *MATCONT*, from Kuznetsov (1995).

<i>Type of object</i>	<i>Label</i>
Point	P
Orbit	O
Equilibrium	EP
Limit cycle	LC
Limit Point (fold) bifurcation	LP
Hopf bifurcation	H
Limit Point bifurcation of cycles	LPC
Neimark-Sacker (torus) bifurcation	NS
Period Doubling (flip) bifurcation	PD
Branch Point	BP
Cusp bifurcation	CP
Bogdanov-Takens bifurcation	BT
Zero-Hopf bifurcation	ZH
Double Hopf bifurcation	HH
Generalized Hopf (Bautin) bifurcation	GH
Branch Point of Cycles	BPC
Cusp bifurcation of Cycles	CPC
1:1 Resonance	R1
1:2 Resonance	R2
1:3 Resonance	R3
1:4 Resonance	R4
Chenciner (generalized Neimark-Sacker) bifurcation	CH
Fold-Neimark-Sacker bifurcation	LPNS
Flip-Neimark-Sacker bifurcation	PDNS
Fold-flip	LPPD
Double Neimark-Sacker	NSNS
Generalized Period Doubling	GPD

Tab. 2.1 Equilibrium- and cycle-related objects and their labels within *MATCONT*

Consider the smooth function f defined in (Eq.2.1). We want to compute a solution curve of the equation $f(x)=0$. Numerical continuation is a technique to compute a consecutive sequence of points which approximate the desired branch. Most continuation algorithms implement a predictor-corrector method. The idea behind this method is to generate a sequence of points x_i , $i = 1, 2, \dots$ along the curve, satisfying a chosen tolerance criterion: $\|f(x_i)\| \leq \varepsilon$ for some $\varepsilon > 0$ and an additional accuracy condition $\|\delta x_i\| \leq \varepsilon'$ where $\varepsilon' > 0$ and δx_i is the last Newton correction.

To show how the points are generated, suppose we have found a point x_i on the curve. Also suppose we have a normalized tangent vector v_i at x_i , i.e. $f(x_i)v_i=0$, $(v_i, v_i)=1$.

The computation of the next point \mathbf{x}_{i+1} consists of 2 steps:

- prediction of a new point,
- correction of the predicted point.

The prediction step detects a first guess \mathbf{X}^0 through the tangent vector \mathbf{v}_i

$$\mathbf{X}^0 = \mathbf{x}_i + h \cdot \mathbf{v}_i \quad (\text{Eq.2.2})$$

Assuming that \mathbf{X}^0 is close to the curve, the point \mathbf{x}_{i+1} on the curve is evaluated through a Newton-like procedure. Since the standard Newton iterations can only be applied to systems with the same number of equations as unknowns, an extra scalar condition has to be added:

$$\begin{cases} f(\mathbf{x}) = 0 \\ g(\mathbf{x}) = 0 \end{cases} \quad (\text{Eq.2.3})$$

The choice of the function $g(\mathbf{x})$ depends on the continuation method adopted. MATCONT uses the Moore-Penrose method.

Let \mathbf{A} be an $N \times (N+1)$ matrix with maximal rank. Consider the following linear system with $\mathbf{x}, \mathbf{v} \in \mathbb{R}^{N+1}, \mathbf{b} \in \mathbb{R}^N$:

$$\begin{cases} \mathbf{A}\mathbf{x} = \mathbf{b} \\ \mathbf{v}^T \mathbf{x} = 0 \end{cases} \quad (\text{Eq.2.4})$$

where \mathbf{x} is a point on the curve and \mathbf{v} its tangent vector with respect to \mathbf{A} , i.e. $\mathbf{A}\mathbf{v} = \mathbf{0}$. The pseudo-inverse (or Moore-Penrose inverse) of \mathbf{A} , which give the least-square solution for the overdetermined system $\mathbf{A}\mathbf{x} = \mathbf{b}$, is

$$\mathbf{A}^+ = \mathbf{A}^T (\mathbf{A}\mathbf{A}^T)^{-1} \quad (\text{Eq.2.5})$$

The solution of (Eq.2.4) is thus $\mathbf{x} = \mathbf{A}^+ \mathbf{b}$, because it fulfill the second condition

$$\mathbf{v}^T \mathbf{A}^+ \mathbf{b} = \langle \mathbf{A}\mathbf{v}, (\mathbf{A}\mathbf{A}^T)^{-1} \mathbf{b} \rangle = 0 \quad (\text{Eq.2.5})$$

since \mathbf{v} is tangent vector of \mathbf{x} with respect to \mathbf{A} . Suppose we have a predicted point \mathbf{X}^0 using (Eq.2.2). We want to find the point \mathbf{x} on the curve which is nearest to \mathbf{X}^0 , i.e. we are trying to solve the optimization problem $\min_{\mathbf{x}} \{\|\mathbf{x} - \mathbf{X}^0\| \text{ s.t. } \mathbf{f}(\mathbf{x}) = \mathbf{0}\}$.

So, the system we need to solve is:

$$\begin{cases} f(\mathbf{x}) = 0 \\ \mathbf{w}^T (\mathbf{x} - \mathbf{X}^0) = 0 \end{cases} \quad (\text{Eq.2.6})$$

where \mathbf{w} is the tangent vector at point \mathbf{x} . In Newton's method this system is solved using a linearization with Taylor expansion about \mathbf{X}^0 :

$$\begin{cases} f(\mathbf{x}) = f(\mathbf{X}^0) + \mathbf{f}_x(\mathbf{X}^0)(\mathbf{x} - \mathbf{X}^0) + o(\|\mathbf{x} - \mathbf{X}^0\|) \\ \mathbf{w}^T (\mathbf{x} - \mathbf{X}^0) = \mathbf{v}^T (\mathbf{x} - \mathbf{X}^0) + o(\|\mathbf{x} - \mathbf{X}^0\|) \end{cases} \quad (\text{Eq.2.7})$$

So when we discard the higher order terms we can see that the solution of this system is:

$$\mathbf{x} = \mathbf{X}^0 - \mathbf{f}_x(\mathbf{X}^0)^+ \mathbf{f}(\mathbf{X}^0) \quad (\text{Eq.2.8})$$

However, the null vector of $\mathbf{f}_x(\mathbf{X}^0)$ is not known, therefore we approximate it by $\mathbf{V}^0 = \mathbf{v}_i$, the tangent vector at \mathbf{x}_i . Geometrically this means we are solving $\mathbf{f}(\mathbf{x}) = \mathbf{0}$ in a hyperplane perpendicular to the previous tangent vector. This is illustrated in Fig. 2.2.

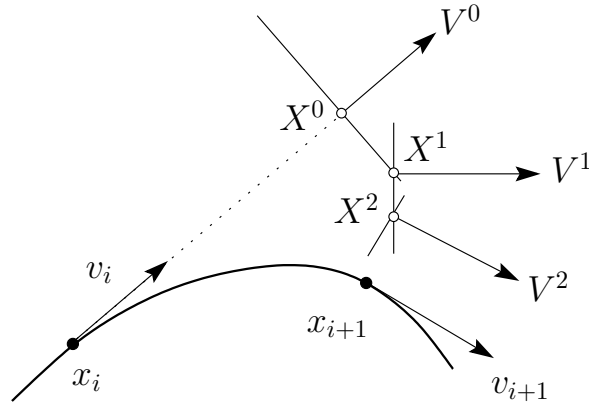


Fig. 2.2 Moore-Penrose continuation, from Kuznetsov (1995).

In other words, the extra function $g(\mathbf{x})$ in (Eq.2.3) becomes:

$$g_k(x) = \langle x - X^k, V^k \rangle \quad (\text{Eq.2.9})$$

where $f_x(X^{k-1})V^k=0$ for $k=1,2,\dots$. Thus, the Newton iteration is:

$$\begin{aligned} \text{iterate} \quad X^{k+1} &= X^k - H_x^{-1}(X^k, V^k)H(X^k, V^k) \\ V^{k+1} &= V^k - H_x^{-1}(X^k, V^k)R(X^k, V^k) \end{aligned}$$

$$\text{with} \quad H(X, V) = \begin{pmatrix} f(X) \\ 0 \end{pmatrix}, \quad H_x(X, V) = \begin{pmatrix} f_x(X) \\ V^T \end{pmatrix} \quad (\text{Eq.2.10})$$

$$R(X, V) = \begin{pmatrix} f_x(X)V \\ 0 \end{pmatrix}$$

One can prove that the Newton iterations expressed in (Eq.2.10) converge to a point on the curve x_{i+1} and the corresponding tangent vector v_{i+1} , respectively, under proper conditions on the step size h and the regularity of f (Jacobian of f not singular).

Obviously this procedure works only for regular points of the curve, since a point which fails the conditions expressed by the Kupka-Smale theorem (a bifurcation) will be singular with respect to some matrix of partial derivatives. To detect the presence of a bifurcation in MATCONT are implemented a set of smooth scalar functions which have regular zeros at the singularity points. These

functions are called test functions. Suppose we have a singularity S which is detectable by a test function $\varphi: R^{n+1} \rightarrow R$. Also assume we have found two consecutive points x_i and x_{i+1} on the curve $f(x)$. The singularity S will then be detected if $\varphi(x_i)\varphi(x_{i+1}) < 0$. Having found two points x_i and x_{i+1} one may want to locate the point x^* where φ vanishes. A logical solution is to solve the following system

$$\begin{cases} f(x) = 0 \\ \varphi(x) = 0 \end{cases} \quad (\text{Eq.2.11})$$

using Newton iterations starting at x_i . However, to use this method, one should be able to compute the derivatives of $\varphi(x)$ which is not always easy. To avoid this difficulty in MATCONT it is implemented by default a one-dimensional secant method to locate $\varphi(x)=0$ along the curve. Notice that this involves Newton corrections at each intermediate point.

2.2 Simulation methods for non-smooth dynamical systems

Let formally introduce a definition for piecewise-smooth dynamical systems.

A piecewise-smooth flow is given by a finite set of ODEs

$$\dot{x} = f_i(x) \quad \text{for } x \in S_i \quad (\text{Eq.2.12})$$

where $\cup_i S_i = DC R^n$ and each S_i has a non-empty interior. The intersection $\sum_{ij} S_i \cap S_j$ is either an R^{n-1} dimensional manifold included in the boundaries ∂S_j and ∂S_i , or is the empty set. Each vector field f_i is smooth in both the state x and the parameters, and defines a smooth flow $\Phi_i(x, t)$, solution of Eq.2.12, within any open set $U \cup S_i$. In particular, each flow Φ_i is well defined on both sides of the boundary ∂S_i .

A non-empty border between two regions \sum_{ij} will be called a discontinuity set, discontinuity boundary or, sometimes, a switching manifold. We suppose that each piece of \sum_{ij} is of codimension one, i.e., is an $(n-1)$ dimensional smooth manifold embedded within the n -dimensional phase space. Moreover, we shall demand that each such \sum_{ij} is itself piecewise-smooth. That is, it is composed of finitely many pieces that are as smooth as the flow (see Fig. 2.3).

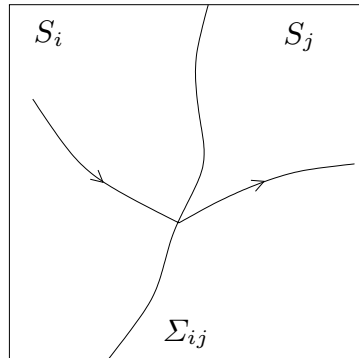


Fig. 2.3 Illustrating schematically trajectories of a piecewise-smooth flow, from Piiroinen and Kuznetsov (2008).

Note that this definition does not uniquely specify a rule for the evolution of the dynamics within a discontinuity set. One possibility is to assign each Σ_{ij} as belonging to a single region S_i only. That is, f_i rather than f_j applies on Σ_{ij} . In fact, such notions make little difference except in the case where the flow becomes confined to the boundary (Filippov trajectories). Before we get to that case, let us first consider what might happen to the flow of the piecewise-smooth ODE as we cross a discontinuity boundary Σ_{ij} .

The degree of smoothness at a point x_0 in a switching set Σ_{ij} of a piecewise-smooth ODE is the highest order r s.t. the Taylor series expansions of $\Phi_i(x_0, t)$ and $\Phi_j(x_0, t)$ with respect to t , evaluated at $t=0$, agree up to terms of $O(t^{r-1})$. That is, the first non-zero partial derivative with respect to t of the difference $[\Phi_i(x_0, t) - \Phi_j(x_0, t)]|_{t=0}$ is of order r .

Now, consider an ODE local to a single discontinuity set Σ_{12} . If f_1 and f_2 differ in an m -th partial derivative with respect to the state x , then the flows Φ_1 and Φ_2 differ in their $(m+1)$ -st partial derivative with respect to t .

Therefore, if $f_1(x) \neq f_2(x)$ at a point $x \in \Sigma_{12}$, then we have degree of smoothness one there. Systems with degree one are said to be of Filippov type. Alternatively if $f_1(x) = f_2(x)$ but there is a difference in the Jacobian derivatives at x , then the degree of smoothness is said to be two. A difference in the second-derivative tensor gives smoothness of degree three, etc. Systems with smoothness of degree two or higher are called piecewise-smooth continuous systems, and we will deal with such systems in the following chapters.

The rigorous numerical analysis of non-smooth dynamical systems remains a theory that is far from complete. When computing solutions to piecewise-smooth systems it is usually not possible to use general-purpose software packages directly, as most black-box numerical integration routines assume a high degree of smoothness of the solution. Accurate numerical computations must make special allowance for the non-smooth events that occur when a discontinuity boundary Σ_{ij} is crossed. Simulation methods for non-smooth systems fall broadly into two categories: time-stepping or event-driven. The former is most often used in many-particle rigid body dynamics, which are high-order

models where there can be perhaps millions of constraints (discontinuities). For such problems, to accurately solve for events of discontinuity boundary crossing within each time-step and to subsequently reinitiate the dynamics would be prohibitively computationally expensive. In contrast, the basic idea of time-stepping is to only check constraints at fixed times at intervals Δt . There are adaptations to standard methods for integrating ODEs that are specifically designed for such systems. Clearly, errors are introduced by not accurately detecting the transition times, and therefore time-stepping schemes are often of low-order accuracy. Several commercially available implementations of time-stepping algorithms are available, especially for the specific case of rigid body mechanics. These often have a variational formulation and are able to deal with the difficult problem of the collision of two rough bodies that may not have unique solutions. See the review by Acary and Brogliato (2008) for more details.

In the following chapters we will deal with low-dimensional systems with a small number of discontinuity boundaries. In that context, explicit event-driven schemes are feasible, fast and accurate. In these methods, trajectories within smooth regions S_i are solved using standard numerical integration algorithms for smooth dynamical systems (e.g., Runge-Kutta, implicit solvers, etc.). Using these methods, the times at which a discontinuity boundary is hit are accurately solved for, and the problem is reinitialized there.

A key requirement for an event-driven method is the ability to define each discontinuity boundary as the zero set of a smooth function $H_{ij}(x)=0$. Also we have to carefully define a set of transition rules at each boundary that applies, if necessary, a reset rule R_{ij} and switches to the integration of a new dynamical system on the far side of the boundary. Thus, the time-integration of a trajectory of the dynamical system is reduced to the finding of a set of event times t_k and events $H_{ij}^{(k)}$ such that $H_{ij}^{(k)}(x(t_k))=0$.

This can be achieved by setting up a series of monitor functions, the values of which are computed during each step of the time-integration. If one of these functions changes sign during a time step, then one needs to use a root finding method to accurately find where $H_{ij}=0$. These ideas have been implemented in Matlab by Piiroinen and Kuznetsov (2008).

One of the main uses of direct numerical simulation is to compute the bifurcation diagrams of the set of attracting solutions directly. In this process, for a fixed parameter value, a set of initial points is chosen and the flow from each point is determined. The flow is computed for a sufficiently long time for transients to decay and for the ensuing dynamics to be deemed to have converged onto an attractor. This dynamics is then recorded, perhaps in a suitable Poincarè section in case of a periodic behaviour of the system. The parameter is then changed slightly and the same process is repeated. However, an even more crucial question is to determine what set of initial conditions to take in order to converge to the various possible attractors. One approach here, which may minimize transient times, is to choose an initial condition for the new parameter value to be a point on the attractor at the previous parameter value. However, such an approach will necessarily miss the possibility of competing attractors present

in the system. Thus, in general one should start from a range of different points within a suitably defined subset D of the phase space from which one has a priori knowledge that the attractors of the system must lie. The number of points should of course be chosen to be as large as possible for the computational time available. One could start with a regular grid of points, but there are advantages in choosing the initial points at random. That is, at each fixed parameter value, use a random number generator to choose initial conditions in D uniformly. This way, the situation where attractors with small basins of attraction are missed consistently at each parameter value are likely to be avoided. We will refer to this method for computing bifurcation diagrams as a Monte Carlo method. The direct simulation method has many advantages in giving a quick and realistic picture of the bifurcation diagram of a system without assuming any a priori structure about the number or form of the attractors.

3 MODELS DESCRIPTION AND ANALYSIS

In this chapter will be described in details the two eco-hydrological models that has been developed. The first model (TGSN) deals with the role of competition between different plant functional types (namely woody and herbaceous plant) for the two most limiting resources in tropical and subtropical biomes (soil moisture and mineral nitrogen). The second model (SNPV) neglect the role of competition in order to address the interaction between the hydrological cycle and the biogeochemical cycle of nitrogen and phosphorous, and the condition for the limitation of nutrient to vegetation growth. The equations of both models are described in details, and their qualitative behaviour is analyzed using the numerical tools described in the previous chapter.

3.1 TGSN model: introduction and bifurcation analysis

A dynamical model of tree-grass-soil water-mineral nitrogen interactions, in a given volume of soil, is introduced here. It describes locally the temporal dynamics of tree and grass in presence of two resources: soil water and mineral nitrogen.

Let z indicate the root zone depth, n the porosity (fractional pore volume), w the control volume having unit area and depth z , $w = 1 \times z$, w_p the pore space in the volume w , $w_p = 1 \times z \times n = 1 \times w_1$, with $w_1 = z \times n$.

The water table is assumed to be deep enough to not affect the water dynamics in the root zone. The dynamics of soil water is described through the mass balance equation of the water present in the control volume relative to the maximum water that can be held in this volume. This dimensionless quantity S ('degree of saturation') ranges in the interval $[0, 1]$. $S=0$ corresponds to completely dry soil, and $S=1$ to completely saturated soil. The soil water balance equation is

$$\frac{dS}{dt} = \frac{P}{w_1}(1 - S) - \varepsilon S - \tau_T ST - \tau_G SG \quad (\text{Eq.3.1})$$

In Eq.3.1, the term P/w_1 represents the rainfall rate normalized with respect to the root zone capacity. Here, P ($P \geq 0$, mm/yr) is assumed constant in the year (i.e, P is the mean annual rainfall). Following De Michele et al. (2008), we assume that the soil surface is more-or-less horizontal, and the whole amount of rainfall infiltrates the soil as long as the soil water holding capacity is not exceeded. The term $P/w_1 S$ models the deep percolation, beyond the rooting zone. When $S=0$ (completely dry soil) all the rainfall contributes to moistening of the root zone. When $S=1$ (saturated root zone) the rainfall runs off or percolates through the soil towards the water table, and it is no longer available to the vegetation at this location. The term εS models the evaporation from the soil. The term $\tau_T ST$ ($\tau_G SG$) models water uptake by the vegetation as proportional to S and the vegetation quantity T (G). The dynamics of the nitrogen are described through the mass balance equation of mineral nitrogen in the soil per unit area, indicated by N ($N \geq 0$, gN/m²):

$$\frac{dN}{dt} = Q - aN - c_T NT - c_G NG \quad (\text{Eq.3.2})$$

In Eq.3.2, Q (gN/m²/yr) is the rate of nitrogen supply. This is principally by mineralization of organic nitrogen in the soil, but also has a component of wet and dry deposition of atmospherically-borne nitrogen and biological nitrogen fixation. In the long term, there is a feedback between the vegetation quantity (T and G) and the amount of soil organic nitrogen that provided the substrate for Q , but the stock of soil organic nitrogen is much bigger than either T or G or the flux Q , so for simplicity this mechanism is subsumed in the net uptake term. a_N is a loss term due to leaching and gaseous losses such as volatilization and denitrification. The nitrogen uptake of plants is represented by two terms proportional to the nutrient mass, and the plant abundance, $c_T NT$ and $c_G NG$, respectively for tree and grass. The consumption of the two resources is a complex combination of simultaneous and independent uptake, since the soil water is both a necessary growth resource and a vehicle for nutrient uptake through water-mediated bulk flow, while the active transport to the xylem and mycorrhizal-mediated transport are independent component of the consumption vector (Gleeson and Tilman 1992). In order to represent this behavior in a simple way, the consumption rates for the inorganic nitrogen are assumed independent of the transpiration rates, but the consumption vectors of both plant forms are not assumed to follow the optimal foraging condition, i.e. that essential resources should be consumed in the proportion for which the population would be equally limited by both resources (Tilman 1982).

The dynamics of vegetation T (G) is described through a mass balance between the growth and the death of vegetation. Here, the growth rate of T (G) is proportional to the consumed water, $w_T \tau_T ST$ ($w_G \tau_G SG$), multiplied by a conversion coefficient η_T (η_G) that depends on the nitrogen content per unit of water uptake (that is, the nitrogen concentration), $c_T NT / \tau_T w_T S$ ($c_G NG / \tau_G w_G S$). According to Larcher (2003), since the plant response to a mineral nutrient depends by its concentration and not by its absolute quantity, we assume that the conversion coefficient η_T (η_G) is zero for scarce values of nitrogen concentration, while it saturates to a maximum when the nitrogen concentration increases according to the Holling II type function,

$$\eta_i = \eta_i^{\max} \frac{\alpha_i c_i N / \tau_i w_i S}{1 + \alpha_i c_i N / \tau_i w_i S} \quad \text{with } i = T, G \quad (\text{Eq.3.3})$$

where α_T (α_G) is a parameter representing the velocity of saturation. We neglect the effect of excessive concentration, leading to depressive effects on growth, since we assume environments characterized by nitrogen scarcity.

The death rate of tree (grass) is proportional to T (G) with a coefficient μ_T (μ_G). In addition, we have a direct effect of tree on the grassy layer, modeled by an additional death rate proportional to TG with a coefficient δ . Thus, the tree dynamics can be expressed as follows:

$$\frac{dT}{dt} = \eta_T^{\max} \frac{\tau_T w_1 \alpha_T c_T S N}{\tau_T w_1 S + \alpha_T c_T N} T - \mu_T T = \phi_T(S, N) T \quad (\text{Eq.3.4})$$

while the grass dynamics is

$$\frac{dG}{dt} = \eta_G^{\max} \frac{\tau_G w_1 \alpha_G c_G S N}{\tau_G w_1 S + \alpha_G c_G N} G - \mu_G G - \delta T G = \phi_G(S, N, T) G \quad (\text{Eq.3.5})$$

The growth functions of tree and grass can be described in term of their isoclines on the S-N plane, particularly the zero growth isoclines (ZGI) that play a crucial role on the stability of the system's steady states. The ZGI present horizontal and vertical asymptotes for the values

$$\left\{ \begin{array}{l} S_T^* = \frac{\mu_T / \eta_T^{\max}}{\tau_T w_1} \\ N_T^* = \frac{\mu_T / \eta_T^{\max}}{\alpha_T c_T} \end{array} \right. \quad \text{and} \quad \left\{ \begin{array}{l} S_G^* = \frac{(\mu_G - \delta T) / \eta_G^{\max}}{\tau_G w_1} \\ N_G^* = \frac{(\mu_G - \delta T) / \eta_G^{\max}}{\alpha_G c_G} \end{array} \right. \quad (\text{Eq.3.6})$$

Fig. 3.1 shows an indicative shape for the ZGI of the two functional types, and taking $T=0$ for the representation of the ZGI relative to the grass. So according to Hypothesis 1, in conditions of low nitrogen but high water availability, ϕ_T has zero growth isocline nearer to the origin than ϕ_G , and the converse is true for high nitrogen, low water conditions. Obviously, the ZGIs under Hypothesis 2 are switched: in conditions of low nitrogen but high water availability, ϕ_G has zero growth isocline nearer to the origin than ϕ_T , and the converse is true for high nitrogen, low water conditions.

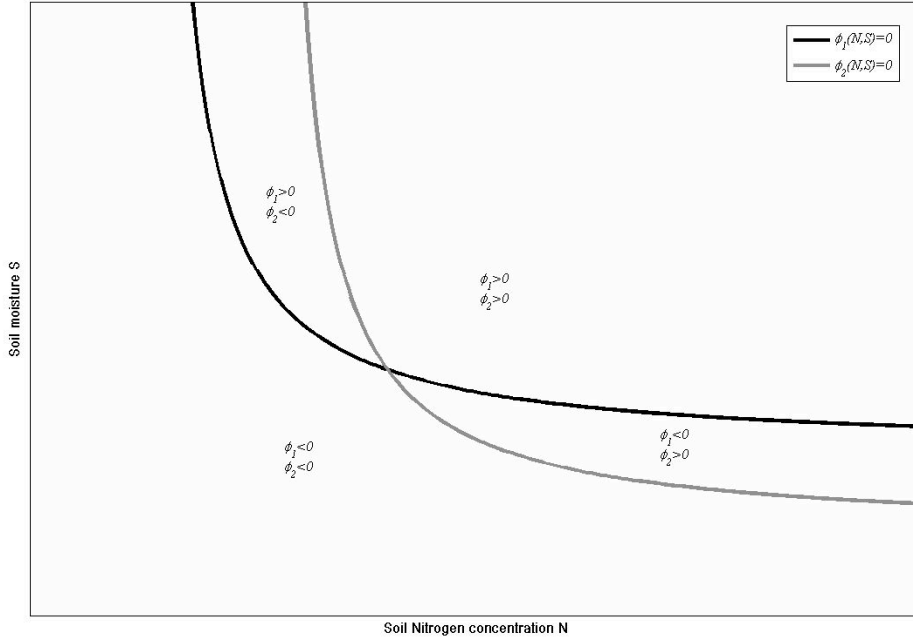


Fig. 3.1 Resource-dependent isoclines for the two functional type. In Hypothesis 1, $\varphi_1=\varphi_T$ and $\varphi_2=\varphi_G$, while in Hypothesis 2 $\varphi_1=\varphi_G$ and $\varphi_2=\varphi_T$.

The interactions among tree-grass-water-nitrogen variables are represented by a fourth order system of non-linear ordinary differential equations:

$$\begin{cases}
 \frac{dS}{dt} = \frac{P}{w_1}(1-S) - \varepsilon S - \tau_T ST - \tau_G SG \\
 \frac{dN}{dt} = Q - aN - c_T NT - c_G NG \\
 \frac{dT}{dt} = \left(\eta_T^{\max} \frac{\tau_T w_1 \alpha_T c_T SN}{\tau_T w_1 S + \alpha_T c_T N} - \mu_T \right) T \\
 \frac{dG}{dt} = \left(\eta_G^{\max} \frac{\tau_G w_1 \alpha_G c_G SN}{\tau_G w_1 S + \alpha_G c_G N} - \mu_G - \delta T \right) G
 \end{cases} \quad (\text{Eq.3.7})$$

Fig. 3.2 shows the nature of the dependencies among the state variables, T, G, S, N.

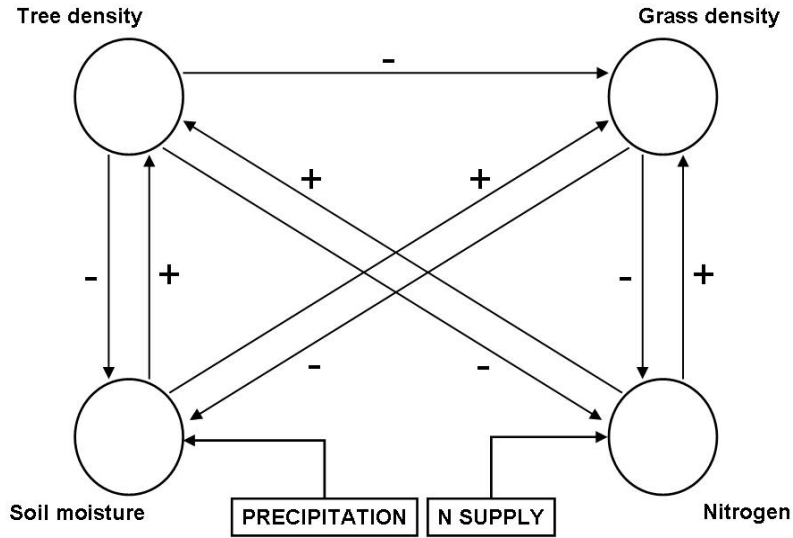


Fig. 3.2 Graph of influences for the state variables.

The steady states are indicated with the symbol “ E ”, and two superscripts q_1q_2 : the first referring to the tree state, and the second to the grass state. Each steady state, $E^{q_1q_2}$, is a 1×4 matrix $E^{q_1q_2} \equiv (S^{q_1q_2}, N^{q_1q_2}, T^{q_1q_2}, G^{q_1q_2})$. Each superscript can be 0 or 1. When a superscript is equal to 0, the correspondent vegetation is *extinct* (i.e., $q_1=0 \Leftrightarrow T=0$, or $q_2=0 \Leftrightarrow G=0$), when a superscript is equal to 1, the correspondent vegetation is *resources controlled*, i.e., one or both of the resources limit the vegetation to a steady state with positive biomass ($q_1=1 \Leftrightarrow T>0$, or $q_2=1 \Leftrightarrow G>0$). Thus, the tree-grass dynamics is conditioned by: 1) the limiting effect of the resources availability, and 2) the limiting effect of the abundance of the conspecific (Keymer et al. 2008). The system described by Eq.3.7 has four steady states. One of these has both q_1 and q_2 equal to 0, representing bare soil, which is a trivial solution for our purposes. The other three solutions, namely E^{01}, E^{10}, E^{11} , represent non trivial vegetation outcomes: resource-limited but treeless grassland, a grassless but resource-limited forest or thicket, and a savanna in which both trees and grass are resource-constrained. The complete set of steady states is summarized in Tab. 3.1.

Symbol	Vegetation	Steady states			
		T	G	S	N
E^{00}	Desert	0	0	$\frac{P/w_1}{\varepsilon + P/w_1}$	$\frac{Q}{a}$
E^{01}	Grassland	0	$\frac{\eta_G^{\max} \tau_G \alpha_G c_G P Q - \mu_G \tau_G a P - \mu_G \alpha_G c_G Q (P/w_1 + \varepsilon)}{\mu_G \tau_G c_G P + \mu_G \tau_G \alpha_G c_G Q}$	$\frac{P/w_1}{\varepsilon + P/w_1 + \tau_G G^{01}}$	$\frac{Q}{a + c_G G^{01}}$
E^{10}	Forest	$\frac{\eta_T^{\max} \tau_T \alpha_T c_T P Q - \mu_T \tau_T a P - \mu_T \alpha_T c_T Q (P/w_1 + \varepsilon)}{\mu_T \tau_T c_T P + \mu_T \tau_T \alpha_T c_T Q}$	0	$\frac{P/w_1}{\varepsilon + P/w_1 + \tau_T T^{10}}$	$\frac{Q}{a + c_T T^{10}}$
E^{11}	Savanna	T^{11}	G^{11}	$\frac{P/w_1}{\varepsilon + P/w_1 + \tau_T T^{11} + \tau_G G^{11}}$	$\frac{Q}{a + c_T T^{11} + c_G G^{11}}$

Tab. 3.1 Steady states of Eq.3.7.

The values for the E^{11} solutions are evaluated numerically because the explicit analytical forms are too complicated. Bifurcation analyses are then performed on the system described in Eq.3.7 in order to identify all the possible behaviors of the dynamical system (Kuznetsov 1995), using the software MatCont2.4 (Dhooge et al. 2006), and considering both the two hypotheses. The following figures give the bifurcation maps respectively for Hypothesis 1 and Hypothesis 2, using as free parameters the two resource supplies P and Q . The exact values of parameters are reported in the caption. Under the case of Hypothesis 1, while the system is in the biologically meaningful domain, i.e. positive supplies and state variables, it presents four transcritical bifurcations (TC) along which the stable solution changes, and a limit point bifurcation (LP), see Fig. 3.3. The transcritical bifurcations are TC1 between E^{00} and E^{10} , TC2 between E^{00} and E^{01} , TC3 between E^{01} and E^{11} , TC4 between E^{10} and E^{11} . The limit point bifurcation is characterized by the vanishing of the equilibrium E^{11} . The P - Q plane is divided in six regions, of which four are characterized by a single stable state: desert (E^{00}) for very small values of precipitation ($P < 250$ mm/y), grassland (E^{01}) when the abundance of mineral nitrogen favors grasses with respect to trees, forest (E^{10}) when the abundance of precipitation favors the growth of trees with respect to grasses, savanna (E^{11}) for values of precipitation and nitrogen which allow the co-existence of trees and grasses. The two remaining regions are characterized by bistability, i.e. the presence of two stable states: grassland and savanna in a region, and grassland and forest in the other. The regions of bistability are due to the abundance of both the two resources which favor both the two equilibria. Then the choice of the equilibrium of the system depends on the initial condition, and on the history of disturbances (Solbrig et al. 1996).

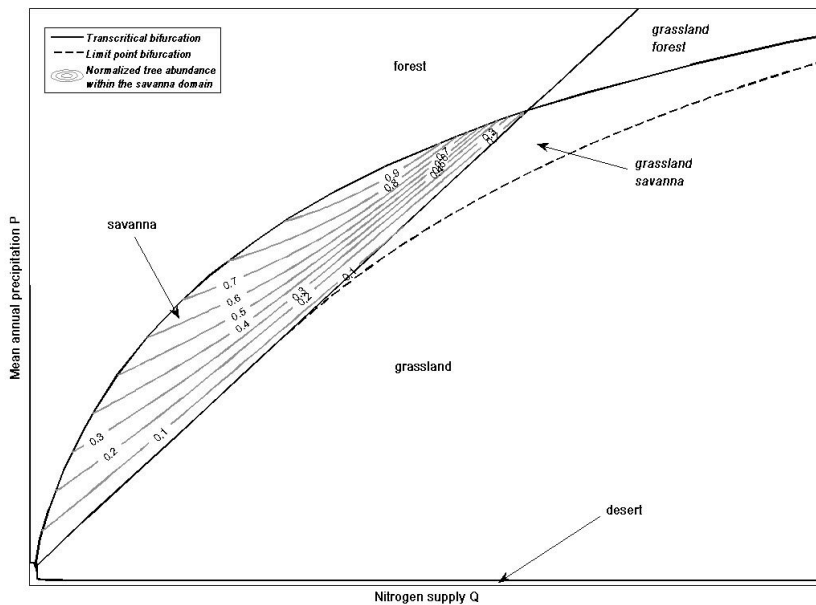


Fig. 3.3 Bifurcation diagram of Eq.3.7 in the plane P - Q and normalized tree abundance within the savanna domain under Hypothesis 1. The values of the fixed parameters are: $w_1=0.35$; $\epsilon=1.2$; $\tau_1=3.6$; $\tau_2=25.0$; $a=0.1$; $c_1=0.3$; $c_2=10.0$; $\eta_1=1.8$; $\eta_2=3.2$; $\alpha_1=5.0$; $\alpha_2=0.05$; $\mu_1=0.3$; $\mu_2=1.35$; $\delta=0.115$.

As highlighted in the formulation of steady states in Tab. 3.1., the direct dependence between the abundance of each functional type at steady state and the two resource supplies allows for obtaining easily the bifurcation map under Hypothesis 2. Switching the role of the two resources, the qualitative shapes of the bifurcations are determined from the map related to Hypothesis 1 operating a reflection in respect to the bisector line of the P - Q plane (Fig. 3.4).

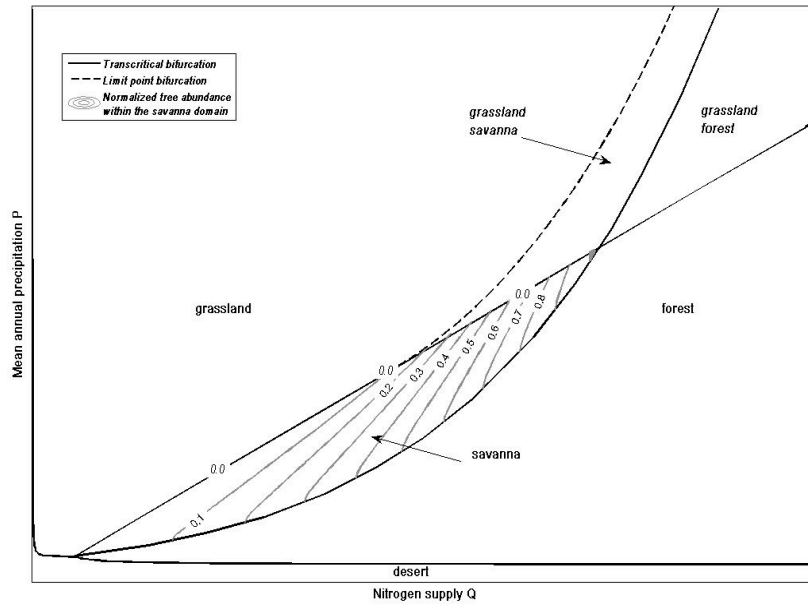


Fig. 3.4 Bifurcation diagram of Eq.3.7 in the plane P - Q and normalized tree abundance within the savanna domain under Hypothesis 2. The values of the fixed parameters are: $w_1=0.35$; $\varepsilon=1.2$; $\tau_1=25.0$; $\tau_2=3.6$; $a=0.1$; $c_1=12.0$; $c_2=0.3$; $\eta_1=1.5$; $\eta_2=2.5$; $\alpha_1=0.05$; $\alpha_2=5.0$; $\mu_1=2.9$; $\mu_2=0.9$; $\delta=2.1$.

The contour lines inside the savanna domain show the behavior of the state variables T , normalized with respect to its maximum value. Under Hypothesis 1, the abundance of trees is increasing under a positive gradient of mean precipitation for a certain level of nitrogen supply, while it decreases with increasing nitrogen for a certain level of mean precipitation. The converse is true under Hypothesis 2. In the following, we use these predictions in order to test the two hypotheses against real data.

3.2 SNPV model: introduction and parameter estimation

In order to characterise the effect of nutrients (N,P) limitation in a theoretical way, we introduce a model that shares the same philosophy of the previous TGSN model: it is minimal by introducing a small set of hypothesis concerning the phenomenon, and it is analitically tractable. The model neglects the influence of competition for resources between different plant functional type, and include the positive influence of moisture condition on decomposition rates of organic matter through mineralization.

The state variables of the model are soil moisture S , concentrations of N and P in the soil and normalized vegetation biomass V . Each equation represents a mass balance for the relative variable with a control volume of unit area and deep equal to the root zone, as in the previous model.

The equations are the following

$$\left\{ \begin{array}{l} \dot{S} = \frac{P}{w_1}(1-S) - \varepsilon S - \tau SV \\ \dot{N} = Q_N + \beta_N S T_N - a_N N - c_N N V \\ \dot{P} = Q_P + \beta_P S T_P - a_P P - c_P P V \\ \dot{V} = [\gamma_S S + \min(\gamma_N N; \gamma_P P)] V (1-V) - \mu V \end{array} \right. \quad (\text{Eq.3.8})$$

The first line describes the water balance in the control volume, corresponding with the relative equation in TGSN model, the only difference being the transpiration term that is now proportional to the average vegetation biomass expressed by V .

The second and third lines represent the mass balance of the two nutrients analyzed, being $a_N N$ ($a_P P$) the loss by leaching through the soil column, $c_N N V$ ($c_P P V$) the uptake by plant, while the first two terms represents the input as a sum between the atmospheric source Q_N (Q_P) and the net mineralization from the total organic pool T_N (T_P), parametrised as a first-order kinetic equation with decomposition rate proportional to the soil moisture $\beta_N S$ ($\beta_P S$), allowing the study of the influence of moisture condition on the concurrent nutrients availability.

In the last line V is the normalized vegetation density, defined by the ratio between the aboveground vegetation density and the maximum value it can reach for a given resource level (its carrying capacity). The dynamics is represented through a modified version of the Tilman equation for meta-populations (Tilman 1982), which derives from the classical logistic equation of intra-specific competition in non-dimensional form

$$\dot{x} = rx(1-x) \quad (\text{Eq.3.9})$$

with growth rate r and normalisation term k (the carrying capacity) defined as

$$\begin{aligned} r &= [\gamma_S S + \min(\gamma_N N; \gamma_P P)] - \mu \\ k &= \gamma_S S + \min(\gamma_N N; \gamma_P P) \end{aligned} \quad (\text{Eq.3.10})$$

The normalisation of vegetation density allows for direct comparison of V with satellite measured indexes of biomass abundance, such as NDVI.

The limiting resource (being either N or P) influences the growth according to the Liebig's law of the minimum leading to a non-smooth dynamical system which is discontinuous in the first derivative. The degree of smoothness is thus two and the system can be classified as piecewise continuous according to the definition given in Chapter 2.2.

The parameter has been estimated by comparison with yearly mass balances at Nysvley site, for the resources equations (S, N, P), while vegetation growth and mortality have been fitted by minimizing the difference between simulated V and mean yearly values of NDVI in the sites listed in the dataset of Sankaran et al. (2005). The dataset contains measurements and estimations of mean annual precipitation, soil physical (texture, bulk density) and chemical (organic soil matter content of nitrogen and phosphorous) characteristics, which were gathered from several sources for a range of sites across Africa. The total number of sites for which precipitation, total nitrogen and phosphorous were available has been splitted in two parts at random. The first part of 63 points has been used for the optimization procedure, while the second part of 58 points is plotted against measured NDVI data for validation in Fig. 3.5.

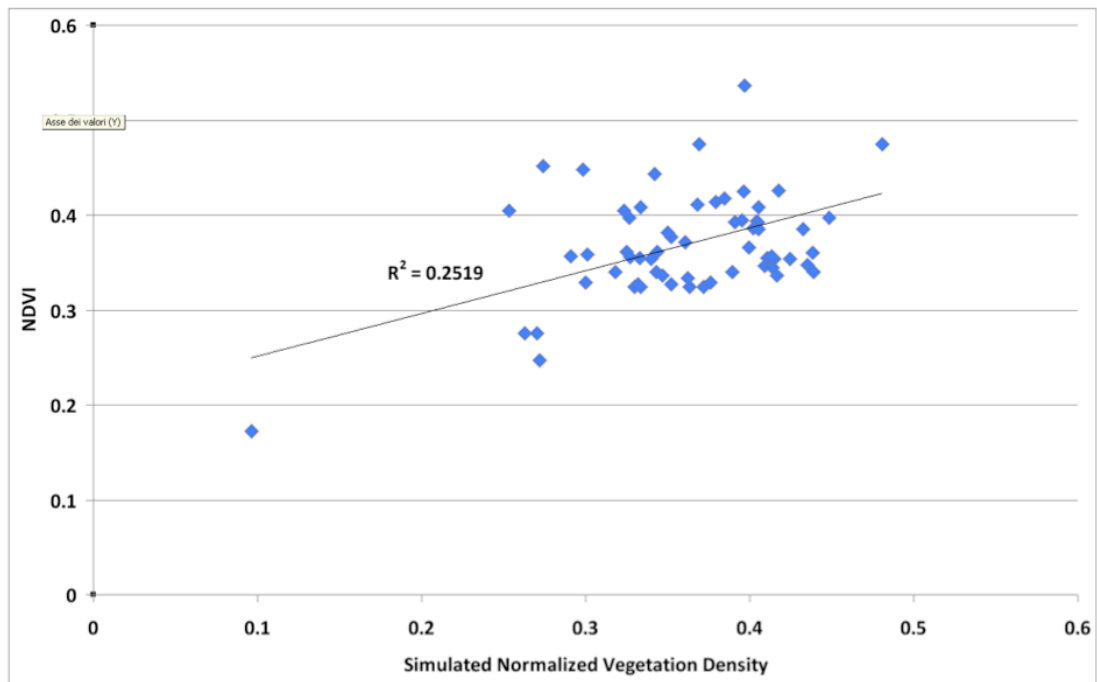


Fig. 3.5 Simulated and measured values of normalized vegetation density after parameter estimation.

From the validation part of dataset it has been calculated some indexes used to address the goodness of the parameter estimation: the linear correlation coefficient, the root mean square error, the mean absolute error and the mean absolute deviation, all reported in Tab. 3.2.

<i>GOF Index</i>	<i>Value</i>
<i>Correlation coefficient</i>	<i>0.502</i>
<i>RMSE</i>	<i>0.059</i>
<i>MAE</i>	<i>0.044</i>
<i>MAD</i>	<i>0.045</i>

Tab. 3.2 Values for goodness-of-fit indexes after parameter estimation.

The values of the parameters after the estimation procedure are listed in the following Tab. 3.3.

<i>Symbol</i>	<i>Name</i>	<i>Unit</i>	<i>Value</i>
w_l	Root zone depth	m	0.35
ε	Evaporation rate	1/yr	0.6
τ	Transpiration rate	1/yr	1.5
q_N	Deposition rate for N	gN/m ² /yr	0.8
β_N	Net mineralization rate for N	1/yr	0.07
a_N	Loss rate for N	1/yr	1.0
c_N	Consumption rate for N	1/yr	4.7
q_P	Deposition rate for P	gP/m ² /yr	0.01
β_P	Net mineralization rate for P	1/yr	0.03
a_P	Loss rate for P	1/yr	0.001
c_P	Consumption rate for P	1/yr	0.25
γ_S	Growth rate for S	1/yr	0.713
γ_N	Growth rate for N	m²/gN/yr	0.324
γ_P	Growth rate for P	m²/gP/yr	0.141
μ	Mortality coefficient	1/yr	0.307

Tab. 3.3 Estimated values for the parameters. Parameters in bold has been estimated by minimizing the difference between simulated V and measured NDVI, the others are obtained according to yearly mass balances of the relevant fluxes and pools at Nylsvley site.

In order to study the influence of the parameters that has been fixed according to site-specific mass balances at Nylsvley, a sensitivity analysis has been carried out on these parameters. Each parameter has been varied from the fixed value according to different levels (or treatments) that are $\pm 10\%$ and $\pm 20\%$ of the fixed value. The variation on the response variable at steady state of the normalized vegetation density has been reported as $\ln(V_x/V)$, with V the response according to undisturbed parameter values, and V_x the response under treatment X.

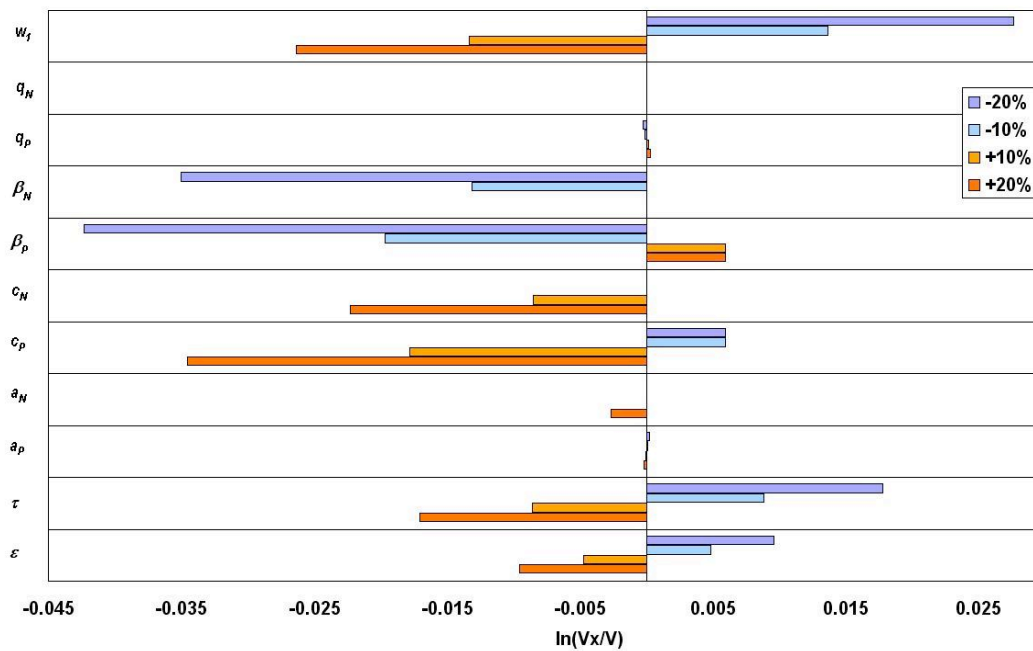


Fig. 3.6 Sensitivity analysis for the parameter estimated according to site specific mass balances at Nylsvley.

The range of variation is within $\pm 1.5\%$ for the greatest part of the parameters. The sensitivity of the model to the parameters governing nutrient losses (a_N , a_P) and atmospheric deposition (q_N , q_P) is the lowest, in agreement with the role of these path in the nutrient cycle, especially for phosphorous. The relatively high sensitivity to variation of root zone depth (w_1) do not represent a drawback to the generality of the model, since this parameter is known for having little variations.

4 DATA COMPARISON AND RESULTS

In this chapter the two models are used in order to address specific eco-hydrological problems. In particular, the problem of the definition of competition status of trees and grasses with respect to soil moisture and nitrogen is addressed in a formal way by using the results from the TGSN model. Furthermore, the model is compared with a global dataset, showing that it can lead to a simple understanding of global patterns of biome distribution in the world.

Finally, the behaviour of the SNPV is analyzed with respect to nutrient enrichment experiments, which represent the main source of observation on the topic of nutrient limitation.

4.1 TGSN model: testing competition status hypotheses

In order to understand if Hypothesis 1 (H1) or Hypothesis 2 (H2) can represent, or not, observed data, we test these two contrasting hypotheses against the dataset described in Sankaran et al. (2005). The dataset contains measurements and estimations of projected woody cover (the percentage of ground surface covered when crowns are projected vertically), MAP, soil characteristics (texture, total nitrogen and phosphorus, and nitrogen mineralization), fire and herbivory regimes, which were gathered from several sources for a range of sites across Africa.

Here we focus the attention on three variables: woody cover, mean annual precipitation and potential N mineralization. This because the woody cover is a proxy of tree abundance; the mean annual precipitation is an indicator of water supply, and the potential N mineralization, quantified following laboratory incubations of soils under anaerobic conditions, is an index of N availability and turnover in soils, a good predictor of the annual N mineralization (Schaffers, 2000). Unfortunately we have not measurements of the model's variables, however we can work with measured values of proxy variables. Here we assume unknown increasing functions between the proxy variables (i.e. woody cover and potential N mineralization) and the model variables (i.e. tree abundance in term of aboveground biomass and annual N mineralization).

In addition we group data, according to the soil type, in sandy, loamy and clayly soil, as estimated through the content of sand and clay. For each soil type, some sections in the P-Q plane are considered in correspondence of fixed values of one resource (precipitation or nitrogen) and selecting all the data points within an interval of size Δ centered in the fixed value. For each vertical (constant nitrogen) and horizontal (constant precipitation) section we estimate the dependence between the woody cover and the other (non-constant) resource. In particular we use the Kendall's τ , which is a non-parametric rank-based measure of association, invariant under monotonic transformations of data (Salvadori et al. 2007), of interest here, because we are working with proxy data. Under the condition of null association (H0), the sampling distribution of Kendall's τ is approximately normal distributed with 0 mean and variance equal to

$$\sigma_{\tau}^2 = \frac{2(2N + 5)}{9N(N - 1)} \quad (\text{Eq.4.1})$$

where N is the sample size. Using this information it is possible to test the independence, or null association, between two variables: if the estimate of τ is out the confidence interval (having the above indicated mean and variance and a level of significance generally assumed equal to 1% and 5%) then

the association is to be considered statistically significant (Press et al. 1992). This test is known as Kendall's test of independence, and considered in the following.

The model, under Hypothesis 1, is characterized by increasing values of woody cover increasing the values of precipitation along vertical sections (i.e. positive values of τ) and by decreasing values of woody cover increasing the values of nitrogen along horizontal sections, (i.e. negative values of τ). Conversely the model under Hypothesis 2 is characterized by $\tau < 0$ along vertical sections, and $\tau > 0$ along horizontal sections.

To investigate the model's behavior, using alternatively Hypothesis 1 (H1) and Hypothesis 2 (H2), against data, we apply the Kendall's test of independence to the sample values of Kendall's τ , between woody cover and resource level (precipitation and nitrogen), for 13 sections identified and reported in Tab. 4.1. In particular,

- for sections at a fixed value of nitrogen, if the sample Kendall's τ is significantly > 0 we can reject H_0 in favor of H1; conversely if τ is significantly < 0 then we can reject H_0 in favor of H2;
- for sections at a fixed value of precipitation, if the Kendall's τ is significantly < 0 we can reject H_0 in favor of H1; conversely if τ is significantly > 0 then we can reject H_0 in favor of H2;

Fig. 4.1 shows the test through box-and-whiskers plots, providing the inter-quartile range (the box) and the 99-percentile range (the whiskers) and the sample estimates of Kendall's τ (the dots) for all the sections considered.

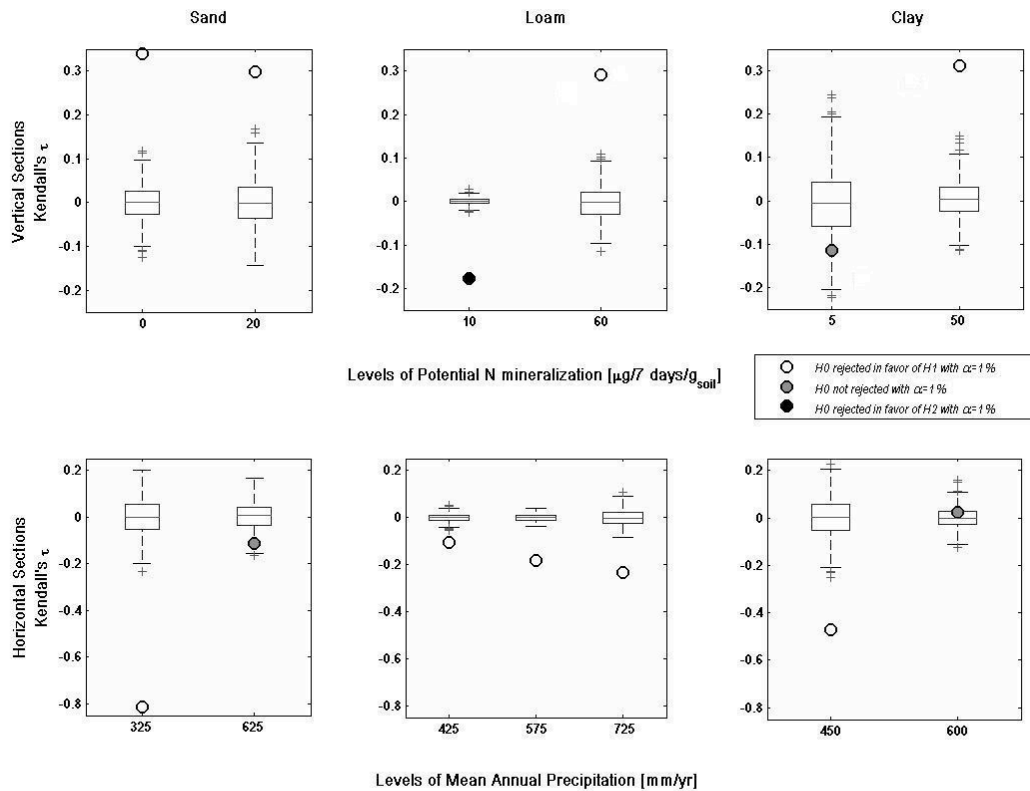


Fig. 4.1 Sample estimates (dots) of Kendall's τ in vertical (top line) and horizontal (bottom line) sections, grouped for soil type. The box-and-whiskers plots represents the sample distributions of Kendall's τ under the hypothesis of null association (H_0).

Tab. 4.1 shows the characteristics of each section (i.e. the level of the fixed resource, the value of Δ , the sample size of grouped data), as well as the results for the test in terms of p-value. The overall performance is presented at the bottom of Tab. 4.1: considering a level of significance of 1%(5%), the results support Hypothesis 1 in the 69% (77%) of cases, Hypothesis 2 in the 8% (8%), and H_0 in the 23% (15%). In order to evaluate the reliability of these findings, we applied the procedure under different configurations (number of sections, width Δ of the bins): the results change from one case to another, but the percentage in favor of Hypothesis 1 remains predominant across the different setups, validating the above presented findings. In the next, we will discharge Hypothesis 2 working with Hypothesis 1 only.

		Sand					Loam					Clay				
	Sec. Num.	Resource Level	Δ	Sample size	p-value: H0vs.H1	p-value: H0vs.H2	Resource Level	Δ	Sample size	p-value: H0vs.H1	p-value: H0vs.H2	Resource Level	Δ	Sample size	p-value: H0vs.H1	p-value: H0vs.H2
Vertical Sections	1	0 ^a	10 ^a	14	<0.01	H0 not rejected	10 ^a	20 ^a	58	H0 not rejected	<0.01	5 ^a	20 ^a	8	H0 not rejected	H0 not rejected
	2	20 ^a		11	<0.01	H0 not rejected	60 ^a		15	<0.01	H0 not rejected	50 ^a		13	<0.01	H0 not rejected
Horizontal Sections	1	325 ^b	100 ^b	8	<0.01	H0 not rejected	425 ^b	75 ^b	30	<0.01	H0 not rejected	45 ^b 0	75 ^b	8	<0.01	H0 not rejected
	2	625 ^b		10	H0 not rejected	H0 not rejected	575 ^b		33	<0.01	H0 not rejected	600 ^b		13	H0 not rejected	H0 not rejected
	3						725 ^b		16	<0.01	H0 not rejected					

^a expressed in $\mu\text{g}/7 \text{ days}/\text{g}_{\text{soil}}$

^b expressed in mm/yr

Total sections:	13	# tests supporting H1:	69% at 1% lev. signif. 77% at 5% lev. signif.	# tests supporting H2:	8% at 1% lev. signif. 8% at 5% lev. signif.	# tests supporting H0:	23% at 1% lev. signif. 15% at 5% lev. signif.
-----------------	----	------------------------	--	------------------------	--	------------------------	--

Tab. 4.1 Testing Hypothesis 1 and Hypothesis 2 vs. data using the Kendall's test of independence.

4.2 TGSN model: validation through a global dataset

To further validate the results of Eq.3.7, we have compared the model's predictions with a global dataset of estimated precipitation statistics, simulated nitrogen supply and classification of biomes. The mean annual precipitation at world scale is derived from the Gridded Climatological Normals (Rudolf et al. 2010, Rudolf and Schneider 2005), provided by the Global Precipitation Climatology Centre [<http://gpcc.dwd.de>]. The dataset focus on the period 1951-2000 and consists of data from ca. 64,400 stations. The climatology comprises normals collected by the World Meteorological Organization, delivered by the countries to GPCC or calculated from time-series of monthly data (with at least 10 complete years of data) available in the GPCC data base. The data processing steps include Quality Control and harmonization of the meta-data (mainly station identification and coordinates), quality-assessment of the precipitation data, selection and intercomparison of the data from the different sources for the particular products, interpolation of the station-related data to a regular mesh system, and calculation of the spatial means on the 1.0° latitude/longitude gridbox area used in the present work.

The nitrogen supply has been obtained by simulations performed using the Community Land Model version 4.0 with Carbon-Nitrogen component (CLM4CN, Oleson et al. 2010) for present day conditions, available on-line [<http://www.earthsystemgrid.org>] from the ESG Gateway at the National Center for Atmospheric Research. The Community Land Model is the land model for the Community Earth System Model, which is a well assessed fully-coupled global climate model extensively used in climate research. The total nitrogen supply has been assumed equal to the mean yearly flux of net nitrogen mineralization, evaluated as functions of proper state variables of the model. The outputs of the model have been filtered to consider only subtropical natural ecosystems. Given the high complexity of such kind of model, we refer to Oleson et al. (2010) for details. Data for fluxes of net nitrogen mineralization has been extracted from the monthly averages of land history data obtained through the offline simulation performed using the Community Land Model version 4.0 with Carbon-Nitrogen component (CLM4CN). The Community Land Model includes processes of biogeophysics (exchanges of energy and momentum between land and atmosphere), hydrology (evapotranspiration, runoff, infiltration, deep drainage), ecology (establishment, survival and competition of vegetation) and biogeochemistry (carbon and nitrogen deposition, mineralization and immobilization). The model calculations are performed over a regular grid with 1.25° of longitudinal resolution and 0.94° of latitudinal resolution. The simulation period is 1948-2004, with atmospheric and land cover data given as transient input and evaluated globally as interpolation of observed data (uncoupled or offline mode). Initial conditions are obtained through a spin-up simulation, that is a simulation of the model under arbitrary initial conditions and constant climatic forcing, until an equilibrium state is reached.

The monthly averages of the state variables are distributed through the ESG Gateway at the National Center for Atmospheric Research [<http://www.earthsystemgrid.org>]. For our purposes, the mean net nitrogen mineralization fluxes of each month of the final year of simulation have been cumulated over the year in order to obtain for each grid cell the yearly net nitrogen mineralization fluxes used in the paper. Only datapoints included in the range of latitude 23.5°S-23.5°N are considered in the present work.

The classification of the different biomes has been obtained by the gridded Global Vegetation Types, 1971-1982 (GVT dataset, see Matthews 1983), available on-line [<http://daac.ornl.gov>] from Oak Ridge National Laboratory Distributed Active Archive Centre. Fig. 4.2 gives the locations of the considered ecosystems.

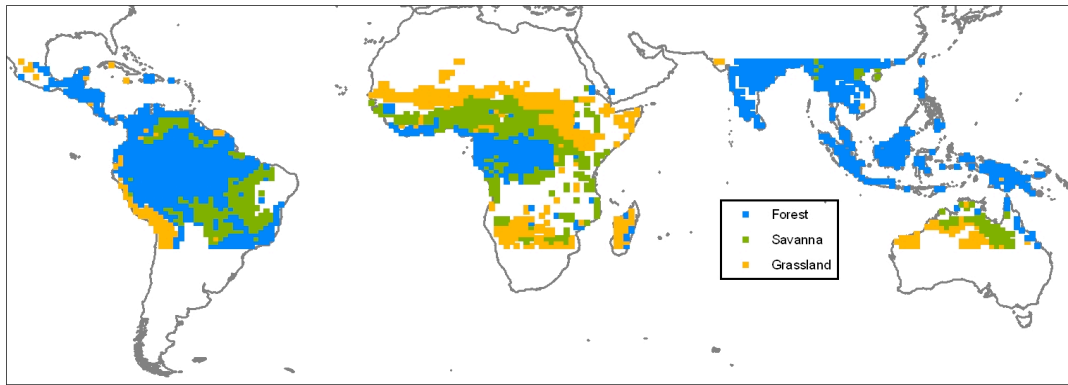


Fig. 4.2 Geographical distribution of the sites considered in the global dataset.

The global vegetation type data of 1.0° latitude/longitude resolution were designed for use in studies of climate and climate change. Vegetation data were compiled in digital form from approximately 100 published sources. The raw data base distinguished about 180 vegetation types that have been collapsed to 32. The vegetation data were encoded using the UNESCO classification system. The classes used in the present work, and the correspondences that have been adopted, are listed in the following

Tab. 4.2.

<i>Class-code in GVT dataset</i>	<i>Description in GVT dataset</i>	<i>Vegetation type</i>
1	tropical evergreen rainforest	Forest (F)
2	trop/subtropical evergreen seasonal broad-leaved forest	
7	tropical/subtropical evergreen needle-leaved forest	
9	tropical/subtropical drought-deciduous forest	
23	tall/medium/short grassland, 10-40% woody cover	Savanna (S)
24	tall/medium/short grassland, < 10% woody cover	
25	tall/medium/short grassland, shrub cover	Grassland (G)
26	tall grassland, no woody cover	
27	medium grassland, no woody cover	
28	meadow, short grassland, no woody cover	

Tab. 4.2 Classes and correspondences adopted within the GVT dataset.

To compare the global dataset with the model we considered as parameters of Eq.3.7 values taken from literature. Tab. 4.3 gives units of measurement and the values of parameters, as long as the references reporting such values. In particular, for the parameters a , c_T , c_G , their values have been obtained accommodating, at yearly scale, the values given by D’Odorico et al. (2003), while for α_T and α_G the values have been chosen in order to obtain tree and grass aboveground biomasses similar to the ones measured in Scholes and Walker (1993) for the broad-leaf *Burkea* savanna at Nylsvley site.

The data of each functional type, with the relative convex hull containing 60% of observations, are plotted against the bifurcation diagram in Fig. 4.3.

Despite some overlapping, it is possible to see how forests, savannas, and grasslands are characterized by values of precipitation and nitrogen supply in agreement with the vegetation regions identified by the bifurcation diagram. Of the 1331 records considered $\approx 72\%$ falls in the vegetation regions predicted by the bifurcation diagram in Fig. 4.3.

<i>Symbol</i>	<i>Name</i>	<i>Range</i>	<i>Value</i>	<i>SI units</i>	<i>Reference</i>
w_1	Root zone depth	0.2-0.5	0.35	m	De Michele et al. (2008)
ε	Evaporation rate	1.0-7.0	5.0	1/yr	De Michele et al. (2008)
τ_T	Water uptake rate for tree	1.0-30.0	3.0	m ² /Kg/yr	De Michele et al. (2008), Klausmeier (1999)
τ_G	Water uptake rate for grass	1.0-30.0	12.0	m ² /Kg/yr	De Michele et al. (2008), Klausmeier (1999)
a	Loss rate of inorganic nitrogen	0.05-0.9	0.1	1/yr	D'Odorico et al. (2003)
c_T	Nitrogen consumption rate for tree	0.1-15.0	0.3	m ² /Kg/yr	D'Odorico et al. (2003)
c_G	Nitrogen consumption rate for grass	0.1-15.0	9.0	m ² /Kg/yr	D'Odorico et al. (2003)
α_T	Saturation coefficient for tree	0.01-10.0	0.5	m/gN	Scholes and Walker (1993)
α_G	Saturation coefficient for grass	0.01-10.0	0.02	m/gN	Scholes and Walker (1993)
η_T^{\max}	Maximum conversion coefficient for tree	1.0-5.0	1.5	Kg/m ³	Klausmeier (1999)
η_G^{\max}	Maximum conversion coefficient for grass	1.0-5.0	3.7	Kg/m ³	Klausmeier (1999)
μ_T	Mortality coefficient for tree	0.1-5.0	0.3	1/yr	De Michele et al. (2008), Klausmeier (1999)
μ_G	Mortality coefficient for grass	0.1-5.0	2.0	1/yr	De Michele et al. (2008), Klausmeier (1999)
δ	Shading coefficient	0.01-0.5	0.07	m ² /Kg/yr	Casagrandi and Rinaldi (1999)

Tab. 4.3 Model's parameters.

In particular the agreement between model and data is 50% in grassland region, 85% in savanna, and 73% in forest. In Fig. 4.4, the comparison between bifurcation diagram and data is shown for continents: Asia and Oceania (left), Africa (center), and Americas (right). In the left panel, $\approx 63\%$ of data falls in the vegetation region predicted by the bifurcation diagram, with the best agreement exhibited by grasslands: 81%. In the African region $\approx 68\%$ of data falls in the vegetation domain predicted by the bifurcation diagram, with the best agreement exhibited by savanna: 95%. In the left panel $\approx 76\%$ of data falls in the vegetation region predicted by the bifurcation diagram, with the best

agreement exhibited by forest: 84%. Note that the agreement between model and data can be improved if one calibrates the model's parameters for the different geographic areas considered.

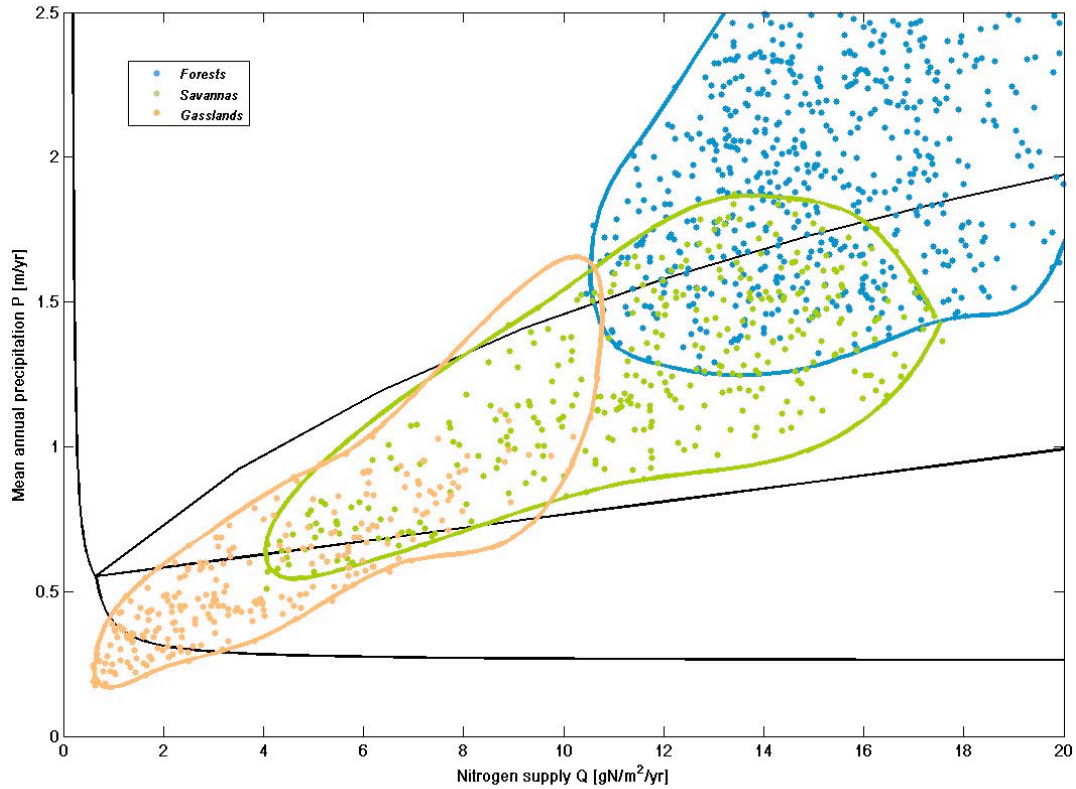


Fig. 4.3 Comparison between model's predictions and the global dataset in the P-Q bifurcation diagram. Grassland (yellow dots), savanna (green dots), forest (blue dots) points, and the relative 60% convex hulls (yellow, green, blue lines).

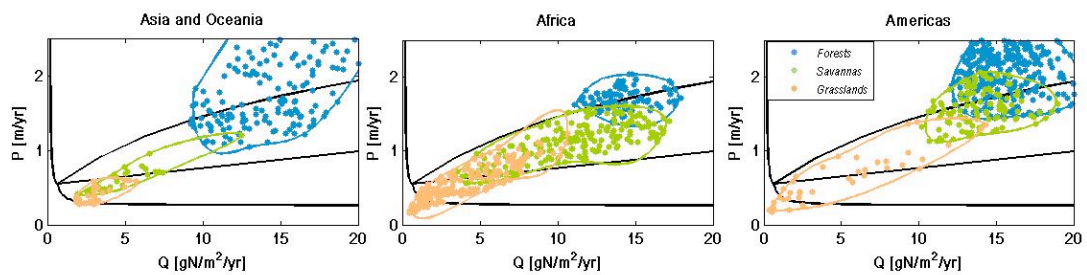


Fig. 4.4 Comparison between the P-Q bifurcation diagram and global dataset divided for continents: Asia and Oceania (left), Africa (center), and Americas (right).

4.3 TGSN model: vegetation dynamics under gradients of resource availability

In order to simulate the ecosystem behavior along resource gradients, we have calculated the equilibrium states of the system after moving the resources along different paths of water and nitrogen supply. We have considered two cases. In the first path P and Q vary linearly according to the equation $P=0.18 Q$, see Fig. 4.5. In the second path, P varies very slowly with Q according to the following linear equation $P=0.006 Q$, see Fig.9. In both figures, panel a) shows the resource path on the bifurcation diagram, panel b) gives the equilibrium states for soil moisture and nitrogen, panel c) illustrates the equilibrium states for tree and grass.

The first path mimics the vegetation structural succession as the rainfall increases from 0 to 2500 mm/yr: desert (no vegetation) → grassland → savanna → forest.

This path qualitatively corresponds to patterns observed in tropical-subtropical environments (see e.g., Walter 1971, Rodriguez-Iturbe and Porporato 2004), where the co-existence of tree and grass occurs in the rainfall range 350-600 mm/yr on nutrient poor soils, and in the range 600-1000 mm/yr on nutrient-rich nitrogen soils.

Note the non-linear decreasing of grass biomass with increasing tree abundance in the region of tree-grass coexistence, due to the combined effect of resource exploitation and direct interaction (shading), as documented in some case studies (Scholes 2003).

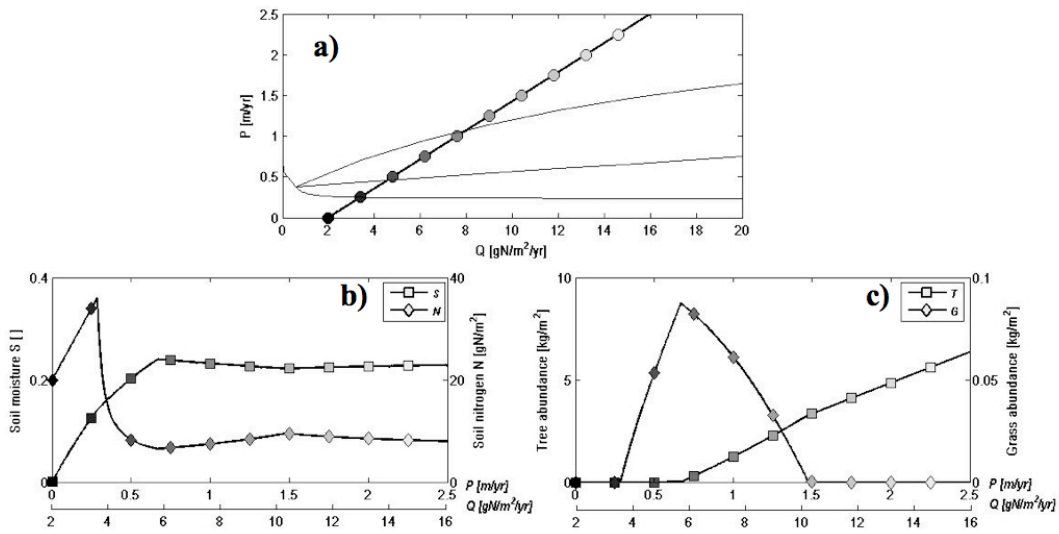


Fig. 4.5 Steady states of tree, grass, soil moisture and mineralized nitrogen along the path $P=0.18 Q$. Panel a) shows the resource path on the bifurcation diagram, panel b) gives the equilibrium states for soil moisture and nitrogen, panel c) illustrates the equilibrium states for tree and grass.

The second path mimics a gradient in soil nitrogen availability, in the middle of the typical savanna rainfall range. It shows the negative dependence between woody abundance and soil nitrogen supply, allowing the shift of the system towards a state of higher grass abundance and even the suppression of the woody layer. Observational support for this result can be found in Sankaran et al. (2008), and for instance, in the striking difference in tree cover between the granitic (low N) and basaltic (high N) soils in the Kruger National park in South Africa (Scholes et al. 2003). Typically, this difference has been ascribed to differences in the fire and herbivory regime, which may still be the case, but this model result shows that other explanations are possible.

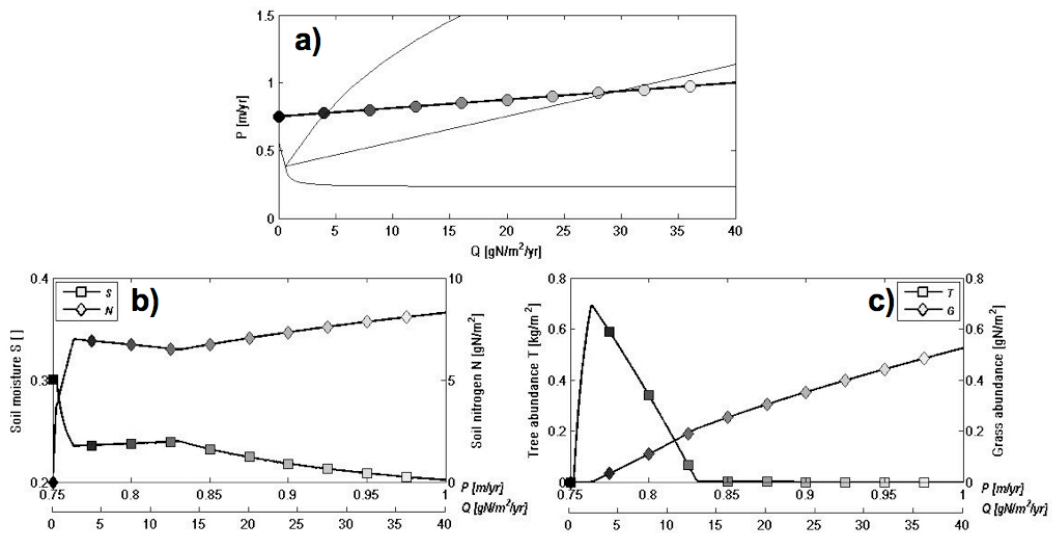


Fig. 4.6 Steady states of tree, grass, soil moisture and mineralized nitrogen along the path $P=0.006 Q$. Panel a) shows the resource path on the bifurcation diagram, panel b) gives the equilibrium states for soil moisture and nitrogen, panel c) illustrates the equilibrium states for tree and grass.

Finally, we show that depending on the ratio between the two resources, one can obtain different scenarios of resource limitation: water to N (low P/Q ratio), N to water (high P/Q ratio), persistent co-limitation for large range of both the resources (intermediate P/Q ratio). These results seem to give some insights to the lack of an ubiquitous pattern of transition between water and nitrogen limitation in arid ecosystems across gradient of resources availability, as shown in different studies of fertilization experiments (Hooper and Johnson 1999).

4.4 SNPV model: analysis of global patterns of nutrient limitation

As highlighted in the introduction, the interaction between N and P limitation in terrestrial ecosystem is still poorly understood, in particular from the point of view of models development. Well assessed biogeochemical models still lack in the representation of the P cycle, thus lacking in the understanding of how P limitation can shapes and influences vegetation in the major biomes of the world.

Starting from our minimal eco-hydrological model, we analyzed its behaviour and the correspondence with results from the research literature available. It has been reported that, in relation with tropical and sub-tropical biomes, P limitation is more frequent in biomes characterized by high productivity (like tropical forest) (Elser et al. 2007). This can be related either to the fact that such biomes lie on more aged soils, or to the feedbacks between moisture and mineralization of nutrients, which are stronger on the N cycle. Thus arid biomes are more interested in N limitation, while in moist ones the increase in mineralization rates of N allows for the switching from N to P limitation.

We extraced 1000 points sampled uniformly from realistic ranges of mean annual precipitation (MAP) and total organic N and P pool sizes (T_N and T_P). With these parameters, that mimic site-specific conditions of precipitation and soil fertility, we performed through SNPV model a simulation for each site until steady state is reached. Then we grouped all the points with the same conditions of nutrient limitation in order to characterize the distribution of MAP values within each group. The results are showed in Fig. 4.7.

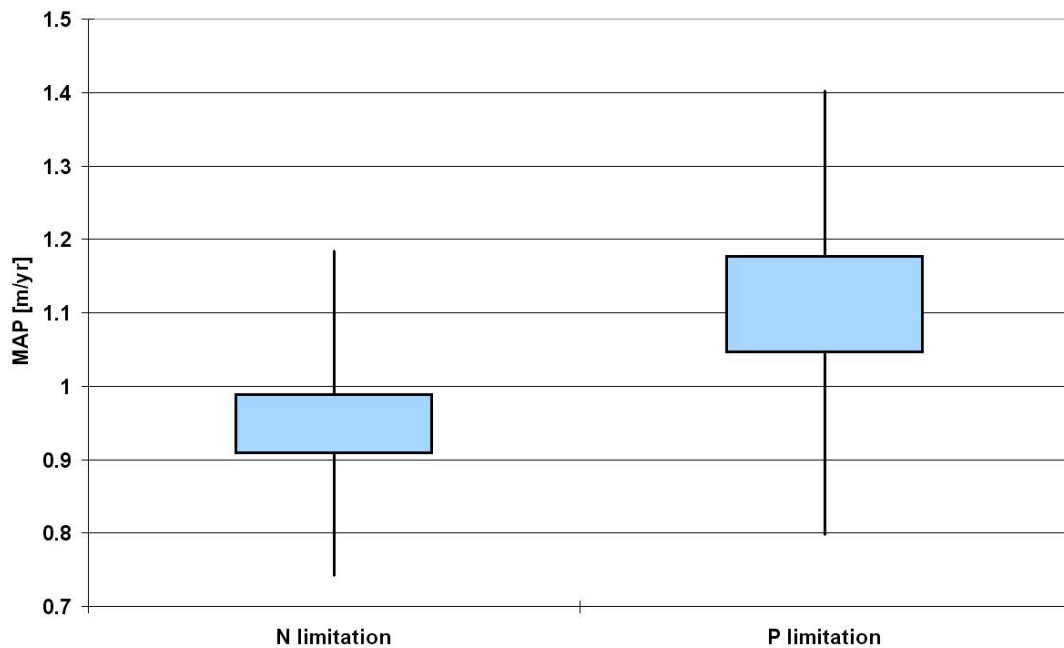


Fig. 4.7 Distribution of MAP values under simulated sites characterized either by N or P limitation. Boxes represent the inter-quartile range, whiskers are the minimum and maximum values obtained

The distribution of MAP under P limiting conditions appears to be shifted toward higher values, and the difference is significant (p -values < 0.001 for a Student's t -test on difference of mean values between the two sample). Thus similar condition of availability of nutrients in soil can lead to different limitation, depending on the precipitation input that influences directly the soil moisture and indirectly the amount of nutrients available for plant via the mineralization process.

The same result come from the representation in the MAP- T_N - T_P space of the boundary between the two limiting condition, that can be obtained through simulation: as showed in Fig. 4.8 and Fig. 4.9, the set of fertility conditions that leads to P limitation become wider as precipitation increases.

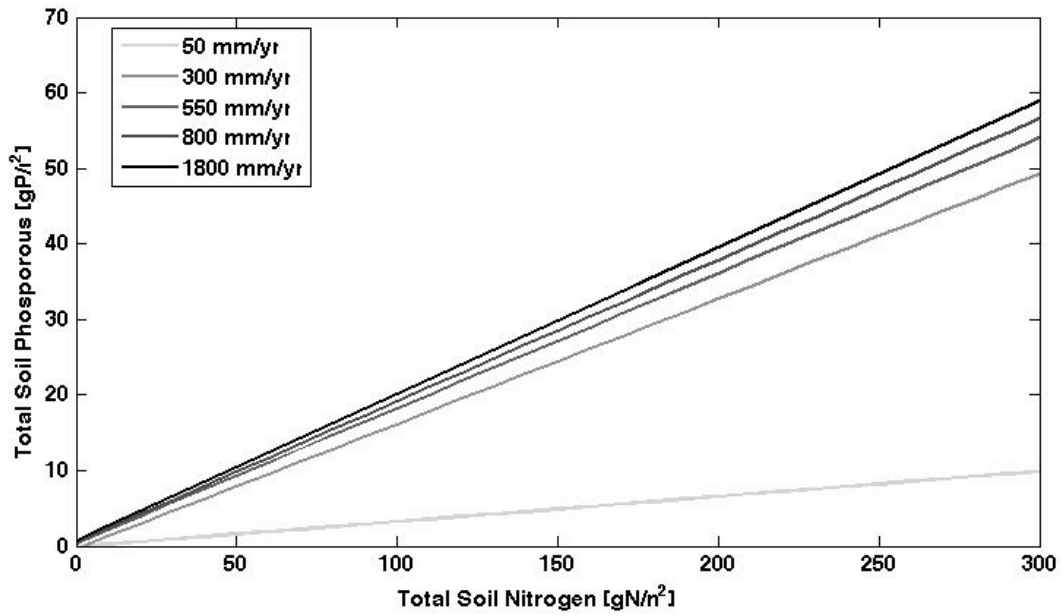


Fig. 4.8 Contour plot of the boundary between N and P limiting conditions for different MAP level.

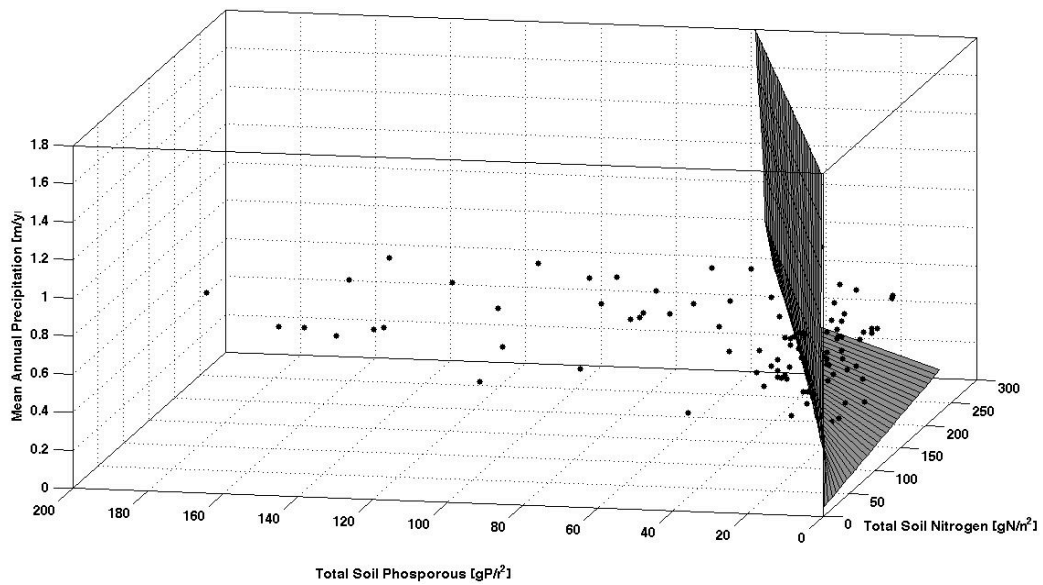


Fig. 4.9 Three-dimensional plot of the boundary between N and P limiting conditions. Points are form the dataset in Sankaran et al. (2005).

Since most of the efforts in studying nutrient limitation has been carried out through nutrient enrichment experiments, we performed the same kind of experiment through model simulation. Base condition of precipitation and soil fertility has been taken from the dataset of savanna sites in Sankaran et al 2005, that has been used for parameter estimation. For each site has been done a simulation until steady state, in order to obtain the values of the response variable V for control. Then a fixed amount of N and P has been added to the equations describing the nutrients dynamics, following three treatments: only N addition (+N), only P addition (+P), combined addition (+N&P). The model has been simulated for further 5 years with initial condition equal to the steady state. The results are expressed in the following Fig. 4.10 in term of $RRx = \ln(Vx/V)$, being Vx the vegetation density obtained after the 5 years simulation with treatment X, and V the control level of the variable. The results has been reported for all the simulated site, then grouped with respect of soil type. The results are similar with those reported in Tripathi et al. (2008), either from a qualitative and a quantitative point of view: they found non significant response to P addition in savanna biome, while for N addition the response is in the range 0.2-0.5, being higher in lower in sand soil and higher in clay soil. It is important to note that our simplified model is influenced by soil type only through the size of the pools of organic N and P, while other aspects (like texture, porosity and infiltration rates) are fixed in the choice of parameter values. Another interesting results from this simulated nutrient enrichment experiment is the size of the response under combined addition, which shows a non-addictive effect of the +N&P treatment, has reported in detail in Allgeier et al. (2010).

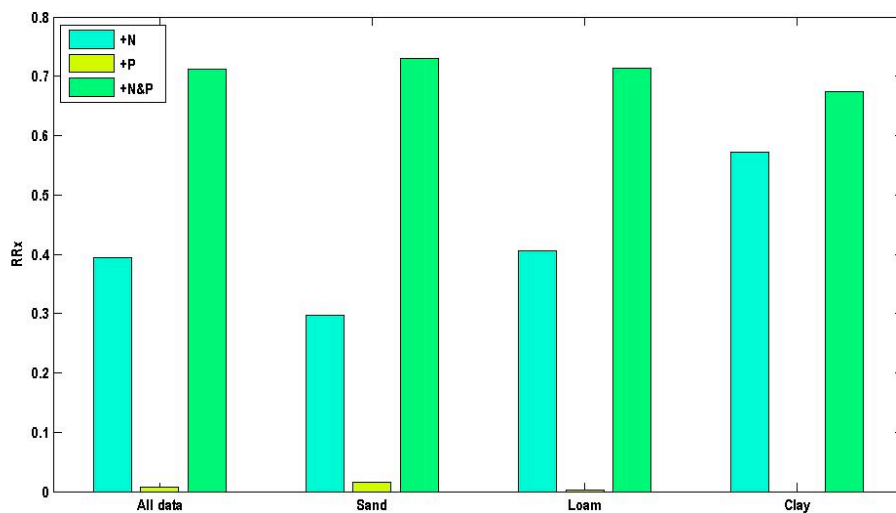


Fig. 4.10 Results from simulated 5-years nutrient enrichment experiments on the savannas site reported in Sankaran et al. (2005).

5 CONCLUSIONS AND FURTHER DEVELOPMENTS

This chapter will resume the main results obtained through the analysis of the two eco-hydrological models developed in the present work. Finally it will be presented some further improvements on the models that are the object of ongoing research activities.

Relevant works that could act as a premise for such activities will be presented. For each improvement will be showed the areas in which it could lead to insights in understanding plant-soil interactions in tropical and subtropical biomes.

One of the main subjects of these ongoing activities are the introduction of the intrinsic stochastic behaviour of rainfall forcing and soil characteristics, which could be represented respectively as random processes and random fields. Also the mineralization of nutrients presents a stochastic nature, since the decay rates of the components of soil organic matter could be modeled in term of proper probability distributions. Finally, taking into account also the influences of fire and herbivory as nutrients sinks as sources could improve the reliability of the models and their prediction capability.

5.1 Insights from TGSN and SNPV model

As stated in the Introduction, the paucity of reliable data at significant time and spatial scales on nutrient dynamics requires a theoretical approach in order to highlight the relevant process and to focus the experimental and modelling effort into proper directions. On the other hand, the extensive use of explicit models that are not linked to data and observations from different disciplines gives results that are poorly explicative, leading to contrasting hypothesis that survive in the literature, as seen in the context of resource competition status. The effort in “filling-the-gap” between different fields of research is crucial if we want to gain a deep understanding of the complex interactions in the biosphere.

The idea here is to address the problem through a theoretical approach, using simple dynamical models as a laboratory to test the behavior of specific ecosystems against data and observations available.

In particular, the TGSN model focused on the role of competition of plant functional types for multiple resources from the soil. Two contrasting hypotheses of competition status, which are supported in the research literature, are discriminated by comparing the predictions of a minimal eco-hydrological mole against data from measurements of soil fertility, climatology and vegetation density from various sites in Africa.

In the context of savanna modeling, a great effort has been taken in order to address the competition between tree and grasses for soil water, however a clear answer about which is the superior competitor for water is yet to be given. The same argument holds with much more strength when we consider the competition for soil nitrogen, issue less studied, presenting difficulties connected to the scarcity of direct and reliable measurements of nitrogen availability at proper spatial and temporal scales, thus limiting the reliability of explicit models (Botter et al. 2009, Everard et al. 2010 for some recent examples).

Our analysis suggests that such ecosystems can be viewed in term of coexistence between tree and grasses permitted by differential strategies adopted by the two dominating functional types with respect to the most limiting resources, that are water and nitrogen. These differential strategies lead trees to be the superior competitor for soil nitrogen, while grasses the superior competitor for soil moisture.

The model’s results are then compared to a global simulated dataset produced by CLM4CN (Oleson et al. 2010). This can be viewed as a comparison with a quite sophisticated model available in literature, a spatially distributed land model covering all the earth surface and including biogeochemical cycles (carbon and nitrogen), vegetation dynamics, land use and river routing (ending with 297 output variables, compared to the 4 state variables of our minimal model. The comparison shows an agreement of about 72%.

The model's results exhibit also successions of vegetation structure along gradients of resources, and in relation to contrasts in soil fertility which match those observed in nature (Hooper and Johnson 1999, Sankaran et al. 2008). Similar results can be seen in Accatino et al. 2010, but translating this behavior in term of biomass rather than coverage needs the inclusion of nutrients as key factors in order to capture the non linearity of tree-grass interactions (Scholes 2003).

In a similar way, but starting with an even poorer quantitative description of the processes involved, the SNPV model tries to analyze the interaction between hydrological and biogeochemical cycles and its role in determining pattern of nutrients limitation. The eco-hydrological model has been developed starting from the equations of soil water balance, nitrogen and phosphorous mineralization-immobilization turnovers. The vegetation dynamics has been represented according to the Liebig's law of the minimum, leading to a non-smooth dynamical system.

The resulting pattern of nutrient limitation has qualitative correspondance with observation of such processes in tropical and subtropical. Simulation of nutrient enrichment on sites with measured values of resource availability are coherent with meta-analysis of real fertilization studies, despite the minimality of the model and the parsimonious parameterization.

These models and their analysis do not solve the debate between equilibrium and disturbance based interpretations of biome distribution, even if they try to clarify, at least for savannas ecosystems, the role of multiple limiting resources in the tree-grass coexistence. Clearly resource competition and disturbance (such as fire and herbivory) are not mutually exclusive, and confirmation or confutation of the presented results will require thoughtful experimentation.

5.2 Ongoing activities

The generality of our eco-hydrological approach in addressing specific topic in biomes ecology could be improved in different ways.

The seasonal and stochastic nature of precipitation and its influence on soil moisture and vegetation dynamics has been studied in De Michele et al. (2008) and Vezzoli et al. (2008). This approach could be incorporated in the TGSN model, giving insights in the role of the timing of nutrient uptake and mineralization, which depend on soil moisture conditions. This is expected to gain relevance in the arid end of the sub-tropical catena, as showed in Scholes et al. 1999 and Williams et al. 2008. An explicit seasonal representation could allow for a comparison with observations of asynchrony between precipitation and nitrogen mineralization, which is documented in Augustine and McNaughton (2004) in some arid savannas and it is thought to be peculiar in subtropical rather than temperate ecosystems.

In the same way, the relevance of disturbances like fire and herbivory in savannas has been showed in De Michele et al. (2011). Taking into account that effect could improve the results of both TGSN and

SNPV model, since those disturbances in turn influence also the nutrient cycling, being either losses (fire) and sources (herbivory) for nutrients.

Another ongoing activity deal with the representation through random fields of the spatial distribution of soil fertility indexes, such as the size of nutrient pools in soil organic matter. This approach could lead to downscaling procedure in order to fill the gap between the spatial scale of global biogeochemical models (>50 km) and those of measurements from the field (<300 m).

An inherent source of uncertainty related to the nutrient cycling come from the mineralization process. The first order kinetics adopted in the SNPV model could be improved by representing the organic matter as a continuum of components characterized by a range of decomposition rates according to proper probability distributions. This approach has been effectively used by Rothman and Forney (2007) in modeling the decomposition of organic matter in oceanic sediments.

References

- Acary V, Brogliato B, 2009. *Numerical Methods for Nonsmooth Dynamics. Application in Mechanics and Electronics*. Springer.
- Accatino F, De Michele C, Vezzoli R, Donzelli D, Scholes RJ, 2010. Tree–grass co-existence in savanna: interactions of rain and fire. *Journal of Theoretical Biology*, 267, 235–242.
- Allgeier JE, Rosemond AD and Layman CA, 2010. The frequency and magnitude of non-additive responses to multiple nutrient enrichment. *Journal of Applied Ecology*, 48 (1).
- Augustine DJ and McNaughton SJ, 2004. Temporal Asynchrony in Soil Nutrient Dynamics and Plant Production in a Semiarid Ecosystem. *Ecosystems*, 7 (8), 829-840.
- Bond WJ and Keeley JE, 2005. Fire as a global ‘herbivore’: the ecology and evolution of flammable ecosystems. *Trends in Ecology and Evolution*, 20 (7), 387-394.
- Botter G, Daly E, Porporato A, Rodriguez-Iturbe I, Rinaldo A, 2008. Probabilistic dynamics of soil nitrate: coupling of ecohydrological and biogeochemical processes. *Water Resources Research*, 44(3), W03416.
- Breman H, de Wit CT, 1983. Rangeland productivity and exploitation in the Sahel. *Science*, 221(4618), 1341–1347.
- Bucini G, Hanan NP, 2007. A continental-scale analysis of tree cover in African savannas. *Global Ecology and Biogeography*, 16(5), 593-605.

Casagrandi R, Rinaldi S, 1999. A minimal model for forest fire regimes. *The American Naturalist*, 153, 527–539.

De Michele C, Accatino F, Vezzoli R and Scholes RJ, 2011. Savanna domain in the herbivores-fire parameter space exploiting a tree-grass-soil water dynamic model. *Journal of Theoretical Biology*, 289, 74-82.

De Michele C, Vezzoli R, Pavlopoulos H, Scholes RJ, 2008. A minimal model of soil water-vegetation interactions forced by stochastic rainfall in water-limited ecosystems. *Ecological Modeling*, 212, 397–407.

Dhooge A, Govaerts W, Kuznetsov YA, Mestrom W, Riet AM, Sautois B, 2006. *Matcont and Cl-Matcont: Continuation toolboxes in Matlab*. Utrecht University, The Netherlands.

D'Odorico P, Laio F, Porporato A, Rodriguez-Iturbe I, 2003. Hydrologic controls on soil carbon and nitrogen cycles. II. A case study. *Advances in Water Resources*, 26(1), 59-70.

D'Odorico P, Laio F, Ridolfi L, 2006. A probabilistic analysis of fire-induced tree-grass coexistence in savannas. *American Naturalist*, 167(3) E79-E87.

Dybzinski R, Tilman D, 2007. Resource use patterns predict long-term outcomes of plant competition for nutrients and light. *American Naturalist*, 170, 305-318.

Elser JJ, Bracken MES, Cleland EE, Gruner DS, Harpole WS, Hillebrand H, Ngai JT, Seabloom EW, Shurin JB, Smith JE, 2007. Global analysis of nitrogen and phosphorus limitation of primary producers in freshwater, marine and terrestrial ecosystems. *Ecology Letters*, 10 (12), 1135–1142.

Everard K, Seabloom EW, Harpole WS, de Mazancourt C, 2010. Plant water use affects competition for nitrogen: why drought favors invasive species in California. *American Naturalist*, 175, 85-97.

Frost PG, Medina E, Menaut JC, Solbrig O, Swift M, Walker BH (eds). 1986. Response of savannas to stress and disturbance. *Biology International Special Issue 10*, IUBS, Paris.

Gebauer RLE, Ehleringer JR, 2000. Water and nitrogen uptake patterns following moisture pulses in a cold desert community. *Ecology*, 81(5), 1415–1424.

Gebauer RLE, Schwinning S, Ehleringer JR, 2002. Interspecific competition and resource pulse utilization in a cold desert community. *Ecology*, 83(9), 2602–2616.

Gleeson SK, Tilman D, 1992. Plant allocation and the multiple limitation hypothesis. *American Naturalist*, 139 (6), 1322-1343.

Hanan NP, Sea WB, Dangelmayr G, Govender N, 2008. Do fires in savannas consume woody biomass? A comment on approaches to modeling savanna dynamics. *American Naturalist*, 171(6), 851-856.

Harpole WS, Suding KN, 2011. A test of the niche dimension hypothesis in an arid annual grassland. *Oecologia*, 166:197-205.

Harpole WS, Tilman D, 2007. Grassland species loss resulting from reduced niche dimension. *Nature*, 446:791-793.

Higgins SI, Scheiter S, Sankaran M, 2010. The stability of African savannas: insights from the indirect estimation of the parameters of a dynamic model. *Ecology*, 91(6), 1682–1692.

Hooper DU, Johnson L, 1999. Nitrogen limitation in dryland ecosystems: responses to geographical and temporal variation in precipitation. *Biogeochemistry* 46, 247–293.

Jansson SL and Persson J, 1982. *Mineralization and immobilization of soil nitrogen*. In: *Nitrogen in Agricultural Soils*. Stevenson FJ (ed.). Agron. Monogr. 22. American Society of Agronomy, Madison, WI.

Jenkinson DS, Andrew SPS, Lynch JM, Goss MJ and Tinker PB, 1990. The Turnover of Organic Carbon and Nitrogen in Soil. *Phil. Trans. R. Soc. Lond. B*, 329 (1255), 361-368.

Keymer JE, Fuentes MA, Marquet PA, 2008. Diversity emerging: from competitive exclusion to neutral coexistence in ecosystems. Santa Fe Institute Working Paper, 08-03-008.

Klausmeier CA, 1999. Regular and irregular patterns in semiarid vegetation. *Science*, 284, 1826-1828.

Kraaij T, Ward D, 2006. Effects of rain, nitrogen, fire and grazing on tree recruitment and early survival in bush-encroached savanna, South Africa. *Plant Ecology*, 186, 235–246.

Kuznetsov YA, 1995. *Elements of applied bifurcation theory*. Springer, New York.

Larcher W, 2003. *Physiological plant ecology: ecophysiology and stress physiology of functional groups* (4th ed.). Springer, New York.

Marschner P and Rengel Z (eds.), 2007. *Nutrient Cycling in Terrestrial Ecosystems*. Springer-Verlag Berlin Heidelberg.

Matthews E, 1983. Global vegetation and land use: new high-resolution data bases for climate studies. *Journal of Climate and Applied Meteorology*, 22, 474–487.

Meyer KM, Wiegand K, Ward D, 2009. Patch dynamics integrate mechanisms for savanna tree–grass coexistence. *Basic and Applied Ecology*, 10, 491–499.

Oleson KW, Lawrence DM, Bonan GB, Flanner MG, Kluzek E, Lawrence PJ, Levis S, Swenson SC, Thornton PE, Dai A, Decker M, Dickinson R, Feddema J, Heald CL, Hoffman F, Lamarque JF, Mahowald N, Niu GY, Qian T, Randerson J, Running S, Sakaguchi K, Slater A, Stockli R, Wang A, Yang ZL, Zeng Xi, Zeng Xu, 2010. Technical Description of version 4.0 of the Community Land Model (CLM). NCAR Technical Note NCAR/TN-478+STR, National Center for Atmospheric Research, Boulder, CO.

Olf H, Ritchie ME, Prins HHT, 2002. Global environmental controls of diversity in large herbivores. *Nature*, 415(6874), 901-904.

Parton WJ, Schimel DS, Cole CV and Ojima DS, 1987. Analysis of Factors Controlling Soil Organic Matter Levels in Great Plains Grasslands. *Soil Science Society of America Journal*, 51 (5), 1173-1179.

Piiroinen PT, Kuznetsov YA, 2008. An event-driven method to simulate Filippov systems with accurate computing of sliding motions. *ACM Transactions on Mathematical Software*, 34 (3).

Press WH, Teukolsky SA, Vetterling WT, Flannery BP, 1992. *Numerical Recipes in C: The Art of Scientific Computing, Second Edition*. Cambridge University Press.

Ricklefs RE, 2008. *The economy of nature*. WH Freeman & Co.

Rodriguez-Iturbe I, Porporato A, 2004. *Ecohydrology of water-controlled ecosystems: soil moisture and plant dynamics*. Cambridge University Press, Cambridge, UK.

Rothman Dh and Forney DC, 2007. Physical Model for the Decay and Preservation of Marine Organic Carbon. *Science*, 316 (5829), 1325-1328.

Rudolf B, Becker A, Schneider U, Meyer-Christoffer A, Ziese M, 2010. GPCP Status Report July 2010.

Rudolf B, Schneider U, 2005. Calculation of Gridded Precipitation Data for the Global Land-Surface using in-situ Gauge Observations. *Proceedings of the 2nd Workshop of the International Precipitation Working Group IPWG, Monterey October 2004, EUMETSAT*.

Salvadori G, Kottegoda N, De Michele C, Rosso R, 2007. *Extremes in nature: an approach using Copulas*. Springer-Verlag New York Inc., New York, NY.

Sankaran M, Hanan NP, Scholes RJ, Augustine DJ, Cade BS, Gignoux J, Higgins SI, Le Roux X, Ludwig F, Ardo J, Banyikwa F, Bronn A, Bucini G, Caylor KK, Coughenour MB, Diouf A, Ekaya W, Feral CJ, February EC, Frost PGH, Hiernaux P, Hrabar H, Metzger KL, Prins HHT, Ringrose S, Sea W, Tews J, Worden J, Zambatis N, 2005. Determinants of woody cover in African savannas. *Nature*, 438(7069), 846-849.

Sankaran M, Ratnam J, Hanan NP, 2008. Woody cover in African savannas: the role of resources, fire and herbivory. *Global Ecology and Biogeography*, 17, 236-245.

Shaffers AP, 2000. In situ annual nitrogen mineralization predicted by simple soil properties and short-period field incubation. *Plant and Soil*, 221, 205-219.

Scholes MC, Martin R, Scholes RJ, Parsons D and Winstead E, 1999. NO and N₂O emissions from savanna soils following the first simulated rains of the season. *Nutrient Cycling in Agroecosystems*, 48 (1-2), 115-122.

Scholes RJ, Walker BH, 1993. *An African Savanna: Synthesis of the Nylsvley Study*. Cambridge University Press, Cambridge, UK.

Scholes, RJ, Hall DO, 1996. The carbon budget of tropical grasslands, savannas and woodlands. In: A.I. Breymer, D.O. Hall, J.M. Melillo & G.I. Agren (eds) *Global Change: Effects on Coniferous Forests and Grasslands*. SCOPE 1996. New York: John Wiley, 69-100.

Scholes RJ, Dowty PR, Caylor K, Parsons DAB, Frost PGH, Shugart HH, 2002. Trends in savanna structure and composition along an aridity gradient in the Kalahari. *Journal of Vegetation Science*, 13(3), 419-428.

Scholes RJ, 2003. Convex relationships in ecosystems containing mixtures of trees and grass. *Environmental and Resource Economics*, 26, 559-574.

Scifres CJ, Mutz JL, Whitson RE, Drawe DL, 1982. Interrelationships of huisache canopy cover with range forage on the coastal prairie. *Journal of Range Management*, 35, 558-562.

Solbrig O, Medina E, Silva J, 1996. Biodiversity and tropical savanna properties: a global view. In: Mooney, H., Cushman, J., Medina, E., Sala, O., Schulze, E. (Eds.), *Functional Role of Biodiversity: a Global Prospective*. John Wiley and Sons Ltd., 185-211.

Teague WR, Smit GN, 1992. Relations between woody and herbaceous components and the effects of bush-clearing in southern African savannas. *Journal of the Grasslands Society Southern Africa*, 9, 60-71.

Tilman D, 1982. *Resource Competition and Community Structure*. Monographs in Population Biology, Princeton University Press.

Tilman D, 1985. The resource-ratio hypothesis of plant succession. *American Naturalist*, 125 (6), 827-852.

Tripathi SK, Kushwaha CP and Singh KP, 2008. Tropical forest and savanna ecosystems show differential impact of N and P additions on soil organic matter and aggregate structure. *Global Change Biology*, 14, 2572–2581.

Vezzoli R, De Michele C, Pavlopoulos H, Scholes RJ, 2008. Dryland ecosystems: The coupled stochastic dynamics of soil water and vegetation and the role of rainfall seasonality. *Physical Review E*, 77 (5).

Walter H, 1971. *Ecology of Tropical and Subtropical Vegetation*. Oliver and Boyd, Edinburgh, UK.

Wang L, D'Odorico P, Reies L, Macko SA, 2010. Patterns and implications of plant-soil $\delta^{13}\text{C}$ and $\delta^{15}\text{N}$ values in African savanna ecosystems, *Quaternary Research*, 73, 77–83.

Wang L, D'Odorico P, O'Halloran Reies L, Caylor K, Macko S, 2010. Combined effects of soil moisture and nitrogen availability variations on grass productivity in African savannas. *Plant Soil*, 328, 95–108.

Whittaker RH, 1975. *Community and ecosystems*. McMillan, New York.

Williams CA, Hanan N, Scholes RJ and Kutsch W, 2009. Complexity in water and carbon dioxide fluxes following rain pulses in an African savanna. *Oecologia*, 161 (3), 469-480.